

European phenological response to climate change matches the warming pattern

ANNETTE MENZEL*, TIM H. SPARKS†, NICOLE ESTRELLA*, ELISABETH KOCH‡, ANTO AASA§, REIN AHASS, KERSTIN ALM-KÜBLER¶, PETER BISSOLLI||, OL'GA BRASLAVSKÁ**, AGRITA BRIEDE††, FRANK M. CHMIELEWSKI‡‡, ZALIKA CREPINSEK§§, YANNICK CURNEL¶¶, ÅSLÖG DAHL|||, CLAUDIO DEFILA***, ALISON DONNELLY†††, YOLANDA FILELLA‡‡‡, KATARZYNA JATCZAK§§§, FINN MÅGE¶¶¶, ANTONIO MESTRE|||, ØYVIND NORDLI****, JOSEP PEÑUELAS‡‡‡, PENTTI PIRINEN††††, VIERA REMIŠOVÁ**, HELFRIED SCHEIFINGER‡, MARTIN STRIZ‡‡‡, ANDREJA SUSNIK§§§§, ARNOLD J. H. VAN VLIET¶¶¶¶, FRANS-EMIL WIELGOLASKI|||, SUSANNE ZACH‡ and ANA ZUST§§§§

*Department of Ecology, Technical University Munich, 85350 Freising, Germany, †NERC Centre for Ecology and Hydrology, Monks Wood, Cambridgeshire PE28 2LS, UK, ‡Central Institute for Meteorology and Geodynamics, 1190 Vienna, Austria, §University of Tartu, 51014 Tartu, Estonia, ¶Swedish Museum of Natural History, 10405 Stockholm, Sweden, ||German Meteorological Service, 63067 Offenbach, Germany, **Slovak Hydrometeorological Institute, 83315 Bratislava 37, Slovak Republic, ††Faculty of Geography and Earth Sciences, University of Latvia, Riga LV-1586, Latvia, ‡‡Faculty of Agriculture and Horticulture, Humboldt-University, Berlin, 14195 Berlin, Germany, §§Biotechnical Faculty, University of Ljubljana, Ljubljana, Slovenia, ¶¶Centre Wallon de Recherches Agronomiques, 5030 Gembloux, Belgium, |||Botaniska Analysgruppen i Göteborg, 40530 Göteborg, Sweden, ***MeteoSwiss, 8044 Zürich, Switzerland, †††Department of Botany, Trinity College, Dublin 2, Ireland, ‡‡‡Center for Ecological Research and Forestry Applications CEAB-CSIC, Universitat Autònoma de Barcelona, 08193 Bellaterra, Catalonia, Spain, §§§Institute of Meteorology and Water Management, 01-673 Warszawa, Poland, ¶¶¶Norwegian University of Life Sciences, 1432 Ås, Norway, |||Instituto Nacional de Meteorología, 28040 Madrid, Spain, ****The Norwegian Meteorological Institute, 0313 Oslo, Norway, ††††Finnish Meteorological Institute, 00101 Helsinki, Finland, ‡‡‡‡Czech Hydrometeorological Institute, Ostrava 70800, Czech Republic, §§§§Environmental Agency of the Republic of Slovenia, Ljubljana, Slovenia, ¶¶¶¶Wageningen University, 6700 AA Wageningen, The Netherlands, |||University of Oslo, 0316 Oslo, Norway

Abstract

Global climate change impacts can already be tracked in many physical and biological systems; in particular, terrestrial ecosystems provide a consistent picture of observed changes. One of the preferred indicators is phenology, the science of natural recurring events, as their recorded dates provide a high-temporal resolution of ongoing changes. Thus, numerous analyses have demonstrated an earlier onset of spring events for mid and higher latitudes and a lengthening of the growing season. However, published single-site or single-species studies are particularly open to suspicion of being biased towards predominantly reporting climate change-induced impacts. No comprehensive study or meta-analysis has so far examined the possible lack of evidence for changes or shifts at sites where no temperature change is observed. We used an enormous systematic phenological network data set of more than 125 000 observational series of 542 plant and 19 animal species in 21 European countries (1971–2000). Our results showed that 78% of all leafing, flowering and fruiting records advanced (30% significantly) and only 3% were significantly delayed, whereas the signal of leaf colouring/fall is ambiguous. We conclude that previously published results of phenological changes were not biased by reporting or publication predisposition: the average advance of spring/summer was 2.5 days decade⁻¹ in Europe. Our analysis of 254 mean national time series undoubtedly demonstrates that species' phenology is responsive to temperature of the preceding

Correspondence: Annette Menzel, tel. +49 8161 714743, fax +49 8161 714753, e-mail: menzel@forst.tu-muenchen.de

months (mean advance of spring/summer by 2.5 days °C⁻¹, delay of leaf colouring and fall by 1.0 day °C⁻¹). The pattern of observed change in spring efficiently matches measured national warming across 19 European countries (correlation coefficient $r = -0.69$, $P < 0.001$).

Key words: climate change, Europe, growing season, meta analysis, phenology, season, temperature response, trend

Received 30 January 2006; revised version received 28 March 2006; accepted 3 April 2006

Introduction

Many studies examining the impacts of global warming on terrestrial ecosystems reveal a consistent pattern of change, the response to warming by phenological change across the northern hemisphere seems to be especially well documented (IPCC, 2001; Sparks & Menzel, 2002; Walther *et al.*, 2002; Parmesan & Yohe, 2003; Root *et al.*, 2003). The majority of the published studies focus on the question of whether changes in systems and sectors relate to changing regional climates. As a consequence of this bulk of studies, further reporting of phenological trends in peer-reviewed journals may become more and more difficult, especially when 'simply' dealing with 'no change' or 'change opposite to the direction expected' (Hughes, 2000; Kozlov & Berlina, 2002; Menzel, 2002). Thus, there exists the danger of reporting or publication bias of these observed impacts. In principle, four combinations of system and climate changes are possible (Fig. 1). 'No change' in the tracking systems seems to be less likely to be reported, especially if it matches with 'no change' in temperatures. However, this combination also emphasises consistency with the functional understanding of the system and predicted climate responses.

Within the Intergovernmental Panel on Climate Change (IPCC), Working Group II on Impacts, Adaptation and Vulnerability is involved with an assessment of observed changes for its next report (AR4, April 2007). Here, it is extremely important to keep track of the

entirety of changes in order to properly address the questions of evidence of no change, change opposite to the direction expected, change not matching climate/temperature change, and to discuss the questions of resilience and thresholds.

Two recent meta-analyses have summarized the coherent picture of a global 'fingerprint' of climate change. Parmesan & Yohe (2003) included multispecies studies from any location that reported neutral, negative and positive results and analysed a total of 677 species or species functional groups' phenology. However, the results of one study site in the United Kingdom (Fitter & Fitter, 2002) alone accounted for nearly half of its records. A second meta-analysis was restricted to publications reporting significant changes of one or many species (Root *et al.*, 2003). Consequently, the average spring advance revealed by the latter was higher (5.1 compared with 2.3 days decade⁻¹). Meta-analyses which include reanalyses of network data for all available species do not yet exist. Thus, the goal of the present study was an exhaustive Europe-wide analysis of all observed changes in phenology (plants/animals) in the period 1971–2000. Owing to the systematic (re-)analysis of all available records, including those from dense phenological networks, this meta-analysis allows, for the first time, a methodical review of absence of evidence and of possible reporting or publication bias. By incorporating monthly temperature series for countries, we were able also to quantify the species' responsiveness to temperature.

		Climate	
		Change	No change
System	Change	Most likely to be published, especially when as expected	Likely to be published, explained by other drivers
	No change	Unlikely to be published, explained by other drivers	Unlikely to be analysed or reported

Fig. 1 Categories of system responses to observed changes and nonchanges in climate and relation to publication biases.

Material and methods

An extremely abundant data set of trends in European phenological phases was systematically collected within the COST action 725 'Establishing a European phenological data platform for climatological applications' (<http://www.cost725.org>) comprising all phenological records digitally available at present. It included entire phenological networks of 11 countries (Austria, Belgium, Czech Republic, Estonia, Germany, Latvia, Poland, Slovakia, Slovenia, Switzerland, Russia (provided by the 5FP project POSITIVE)), five specialists networks (Finland, Spain, the Netherlands, Norway,

United Kingdom) and the network of the International Phenological Gardens in Europe (http://www.agrar.huberlin.de/pflanzenbau/agrarmet/ipg_en.html), spreading over 14 countries including, in addition to countries named above, Croatia, Denmark, Greece, Ireland and Macedonia. In total, phenological trends of 542 plant species in 21 countries (125 628 time series) and 19 animal species in three countries (301 time series) were analysed. The phenophases of wild plants, fruit trees and agricultural crops were assigned to a BBCH (Biologische Bundesanstalt, Bundessortenamt and CHemical Industry) code (Meier, 1997) and grouped either by BBCH code or BBCH subgroups (principal growth stages). If applicable, agricultural and natural phases were treated separately.

Annual mean onset dates for nine countries (Austria, Belarus/northern Russia, Estonia, Czech Republic, Germany, Poland, Slovenia, Switzerland, Ukraine/southern Russia), comprising 254 records (phenophases \times countries) of 10+ years, however, mostly covering the total period 1951–1999, were available for the quantitative assessment of temperature responses. Annual, monthly and seasonal temperature means for all European countries (1901–2000) were used from the Tyndall Centre (Mitchell *et al.*, 2002, 2004).

Annual mean onset dates were correlated by Pearson's product moment correlation with three mean monthly temperatures (the month of mean onset, and the two preceding months) of the respective country. The highest correlation coefficient of these three served as a measure for the temperature responsiveness of the respective phenophase in that country. The slopes of linear regressions of the annual mean dates against the mean temperature of the month before the event provided a measure for the temperature sensitivity. These regression coefficients were analysed in total, by mean onset date, by phenophase group and for selected species \times country combinations.

Each of the COST725 team member states contributed a countrywide trend analysis (1971–2000) including mean onset dates and their standard deviation, linear regressions of the onset dates against year including slope of the regression, standard error of the slope and significance of the regression by *F*-test. In the subsequent meta-analysis (103 199 records of 15+ years) these trends were analysed for Europe by four phenophase groups (b0, farmers' activities; b1, flowering and leaf unfolding; b2, fruiting; b3, leaf colouring), for countries by phenophase groups, and for countries and species.

Results

We found that phenological changes were a clear reaction to temperature. Figure 2a displays all correlation coefficients of 254 mean national records with tempera-

ture. Most phases correlated significantly with mean monthly temperatures of the month of onset and the two preceding months. For 19% of the phenophases the highest correlation was with the month of onset, 63% with preceding month and 18% with 2 months earlier. The average correlation coefficients for four groups (farmers' activities, spring and summer phases, fruit ripening, leaf colouring) are given in Table 1; their means all clearly differed from 0 (*t*-tests, b0–b2 $P < 0.001$, b3 $P < 0.007$). Analysis of variance followed by Tukey's HSD showed that there were significant differences ($P < 0.001$) between the groups in their average correlation with temperature, all of which differed from one another except farmers' activities and fruit ripening.

For spring and summer, and most of the autumn fruit ripening phases, the mean correlation coefficient was negative. Thus, higher temperatures were related to earlier onset dates. The mean value for flowering (Fig. 2a, $\bar{r} = -0.69$) and other spring phases, such as leaf unfolding and budburst of wild plants ($\bar{r} = -0.69$), shooting and closure of the stands ($\bar{r} = -0.62$) as well as ear formation ($\bar{r} = -0.55$) of agricultural crops displayed quite similar temperature sensitivity. Farmers' activities, such as drilling, tilling, harvesting, known as 'false phases', which respond to a lesser degree to climate, also revealed a quite high mean correlation with temperature ($\bar{r} = -0.53$). Only the emergence and sprouting of agricultural winter crops in autumn, which is very much related to harvesting and subsequent drilling, were less related to temperature ($\bar{r} = -0.28$). Earlier fruit ripening was connected to warmer summers ($\bar{r} = -0.45$); only for *Aesculus hippocastanum* in Switzerland and Slovenia was there an opposite relationship. Fruit ripening of agricultural plants was more closely related to temperature ($\bar{r} = -0.57$) than wild plants ($\bar{r} = -0.29$). Delayed leaf colouring was associated with higher temperatures ($\bar{r} = +0.33$); only in eastern Europe (Russia-Belarus, Russia-Ukraine and Czech Republic) did warming result in earlier leaf colouring. There was a clear dependence of the temperature sensitivity on mean timing as earlier phases and very late phases had the highest correlation, negative and positive, respectively, with temperature.

The temperature response was assessed by the slope of linear regression of mean date on mean temperature of the month before onset (Fig. 2b). Spring and summer phases advanced by up to 4.6 days $^{\circ}\text{C}^{-1}$ warming (two outliers in summer are related to agricultural phases in Germany) and autumn leaf colouring was delayed by up to 2.4 days $^{\circ}\text{C}^{-1}$. Overall, mean onset dates influenced the temperature response, the mean for autumn phases (+0.98 days $^{\circ}\text{C}^{-1}$) did differ significantly from the other three groups' means (-2.10, -2.52 and -2.18

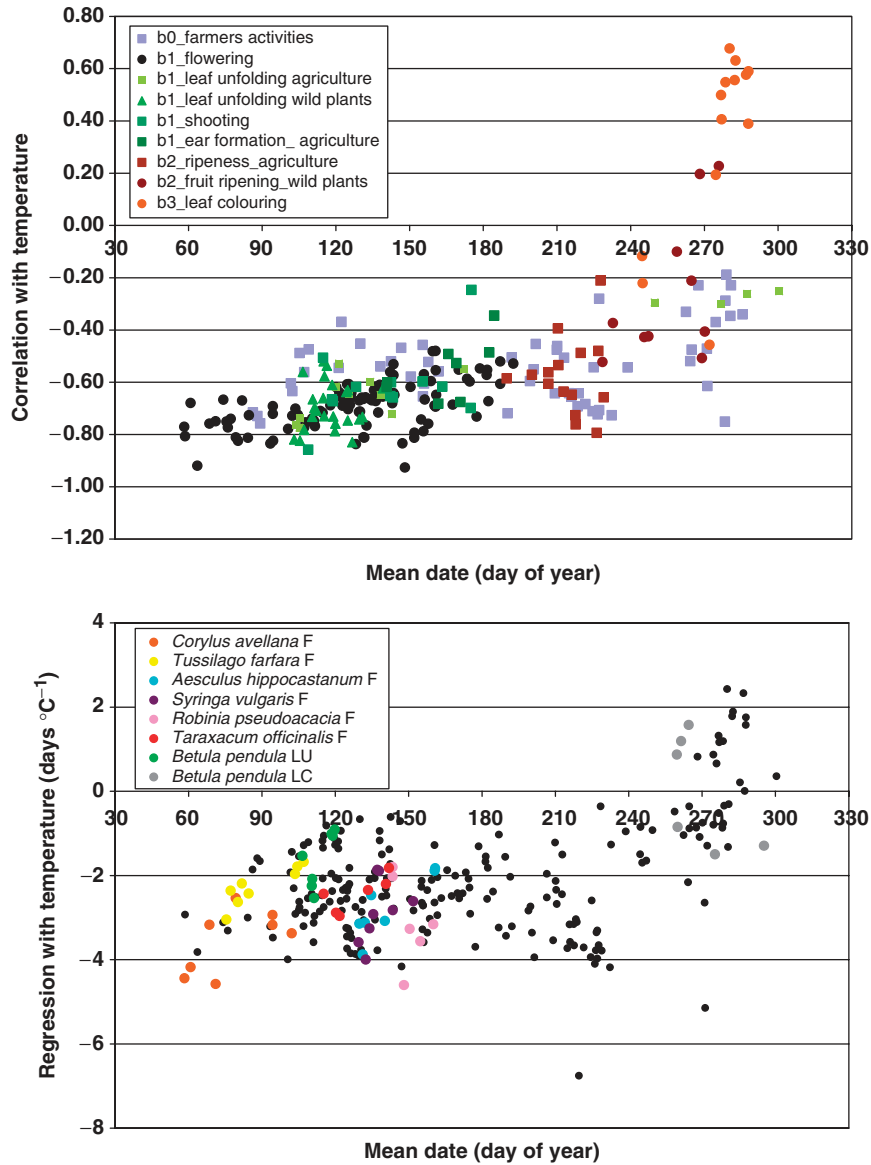


Fig. 2 Temperature sensitivity and response across the year. (a) Maximum correlation coefficients of 254 mean national time series in nine European countries (see ‘Material and methods’) with mean temperatures of the previous months. Phenophases groups include farmers’ activities (b0), spring and summer with different leafing, shooting and flowering phases (b1), autumn fruit ripening (b2) and leaf colouring of deciduous trees in fall (b3). (b) Regression coefficients against mean temperature of the previous month. F, flowering; LU, leaf unfolding; LC, leaf colouring. The overall dependence of temperature sensitivity and response on mean date is high (a) $R^2 = 0.59$, $y = 0.0000003x^3 - 0.0001204x^2 + 0.0182684x - 1.5823$, $P < 0.001$; (b) $R^2 = 0.47$, $y = 0.0000024x^3 - 0.0011345x^2 + 0.170218x - 10.4650$, $P < 0.001$).

days °C⁻¹) (Table 1). Phases analysed for more than six countries are highlighted in Fig. 2b: All spring phases, except *Robinia pseudoacacia* flowering, exhibited a stronger response to temperature in warmer than in colder countries. The regression coefficients of the temperature sensitivity against mean onset date of flowering (days °C⁻¹ per day of the year) were 0.028 ($R^2 = 0.37$) for *Corylus avellana*, 0.030 ($R^2 = 0.78$) for *Tussilago farfara*, 0.047 ($R^2 = 0.74$) for *A. hippocastanum*, 0.049 ($R^2 = 0.21$)

for *Syringa vulgaris*, 0.029 ($R^2 = 0.60$) for *Taraxacum officinale*, and, in contrast, -0.072 ($R^2 = 0.21$) for *R. pseudoacacia*. For *Betula pendula*, both the rate of advance of leaf unfolding and the rate of delay of leaf colouring per °C temperature rise were also higher in (warmer) countries with earlier mean onset (regression coefficients 0.093, $R^2 = 0.54$ and -0.062, $R^2 = 0.40$, respectively).

All observed changes in Europe (1971–2000, 103 199 time series with 15 + years) are summarized in Table 2

Table 1 Mean temperature sensitivity and response of phenological phases

Phenophase group		<i>n</i>	Mean ± SE of correlation coefficient	Mean ± SE of regression coefficient
b0	Farmers activities	54	-0.53 ± 0.02	-2.10 ± 0.16
b1	Leaf unfolding, flowering	160	-0.66 ± 0.01	-2.52 ± 0.07
b2	Fruit ripening	25	-0.45 ± 0.05	-2.18 ± 0.34
b3	Leaf colouring	13	+0.33 ± 0.10	+0.98 ± 0.37

Correlation and regression coefficients (slopes) of annual mean phenological records for nine European countries (see 'Material and methods') against mean monthly temperatures of the respective country (the month of mean onset, and the two preceding months); (see 'Material and methods').

Table 2 Summary of phenological trends in Europe

Phenophase group		<i>n</i>	Neg_all	Neg_sig	Pos_all	Pos_sig	Tr _{mean}	avTr _{mean}
b0	Farmers activities	22338	0.57	0.13	0.43	0.06	-0.041	-0.060
b1	Leaf unfolding, flowering	64027	0.78	0.31	0.22	0.03	-0.250	-0.200
b2	Fruit ripening	11191	0.75	0.25	0.25	0.03	-0.237	-0.190
b3	Leaf colouring	5643	0.48	0.12	0.52	0.15	0.017	0.129
b1 + b2	Leaf unfolding, flowering, fruit ripening	75218	0.78	0.30	0.22	0.03	-0.248	-0.198

All temporal trends (1971–2000, time series of 15 + years) which have been systematically reported to the COST725 meta-analysis (*n* = 103 199) for four different groups. Neg_all/Pos_all proportions of negative and positive trends, Neg_sig/Pos_sig proportions of significantly negative and positive trends (*P* < 0.05), Tr_{mean} mean slopes for Europe (days yr⁻¹), avTr_{mean} average of national mean slopes (days yr⁻¹) to adjust for different station numbers in the different national networks.

by sign, significance, and means of the trends. In general, for farmers' activities and especially spring, summer, as well as fruit ripening phases, there were more negative than positive trends (i.e. more time series revealed advancing onset), in contrast to leaf colouring and leaf fall phases where we had almost the same proportion of negative and positive trends (Fig. 3). Thus, there is a clear signal across Europe of changing spring and summer phenology with 78% of leaf unfolding and flowering records advancing (31% significantly) and only 22% delayed (3% significantly). The signal in farmers' activities was generally smaller (57% advancing, 13% significantly, 43% delayed, 6% significantly). In contrast to spring events, the signal for leaf colouring in fall is quite ambiguous (48% advancing, 52% delayed) and less apparent as there were similar proportions of negative and positive significant trends. It is important to note that fruit ripening of different species was mostly advanced (75% negative, 25% significantly negative; 25% positive, 3% significantly positive trends). The total signal for spring and summer phenology including fruit ripening of wild plants was apparent with almost 80% advancing time series. These results strongly support previous results on a smaller number of sites and species and confirm them as being free from bias towards reporting global change impacts. Average trends in farmers' activities were small (Table 2), while those of leafing, flowering and fruiting show a

clear advance of 2.5 days decade⁻¹. Leaf colouring and fall trends were close to 0, but suggested more of a delay when the average trend per country is examined (1.3 days decade⁻¹).

When analysing the country means of the trends we found, for the first time, that phenology is not only a good bio-indicator for temperature changes in general, but also mirrored them quantitatively. Average phenological trends for countries systematically varied with temperature changes of the same country. Thus, for spring, our analysis revealed higher negative (advancing) trends of flowering and leaf unfolding in countries which exhibit a stronger warming in the preceding month (1971–2000; *r* = -0.69, *P* < 0.001, 19 countries, Fig. 4a). Even the average trends of animal spring phases in three countries fitted perfectly into the relationship between phenological and temperature trends. Mean fruit ripening trends in eight European countries matched national temperature changes of the previous month quite well (*r* = -0.66, *P* = 0.076, Fig. 4b). For leaf colouring and leaf fall in autumn, there is no clear relationship between national phenological and temperature trends (*r* = 0.003, *P* = 0.99, 14 countries, Fig. 4c). Even for single species, such as leaf unfolding of *Fagus sylvatica* and flowering of *Prunus avium*, their mean national trends match the pattern of temperature increase in March (*F. sylvatica* *r* = -0.86, *P* = 0.003, nine countries, Fig. 4d; *P. avium* *r* = -0.73, *P* = 0.004, 13 countries, Fig. 4e).

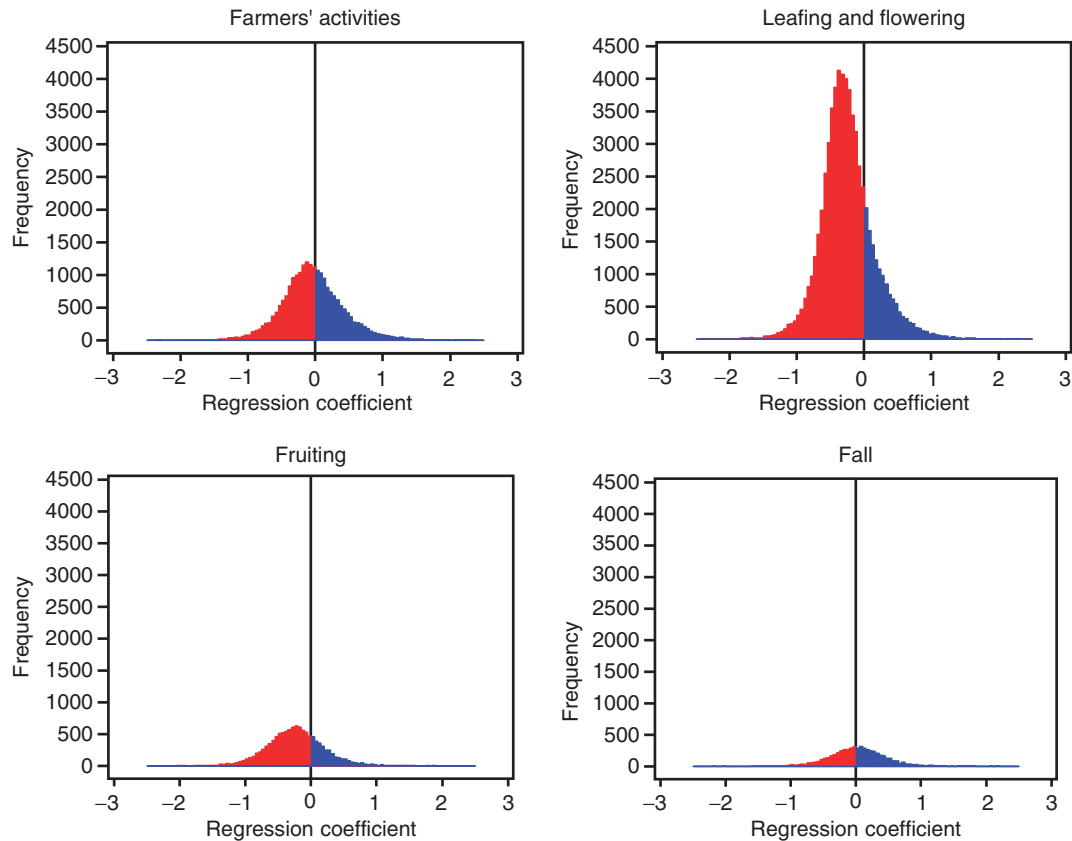


Fig. 3 Histograms of phenological trends in Europe. All temporal trends (1971–2000, time series 15+ years) as linear regression coefficients (days yr^{-1}) systematically reported to the COST725 meta-analysis ($n = 103\,199$) for four different groups.

Discussion

Our meta-analysis comprised a huge selection of species and countries, included false phases in farming, and various phases of wild and agricultural plants covering the whole vegetation period. Owing to the enormous number of records included, the results are representative for Europe. The temperature response of spring phenology was unquestionable. We found that the earlier species were more sensitive, probably because of higher temperature variability in spring months, and they better indicated changes in temperature. The autumn signal was vague (delayed leaf colouring, but earlier fruit ripening because of warming, the latter more pronounced in agricultural than wild plants), thus further studies about observed climate change impacts in autumn should clearly differentiate between these phases. The temperature response varied between $-4.6 \text{ days } ^\circ\text{C}^{-1}$ in spring and $+2.4 \text{ days } ^\circ\text{C}^{-1}$ in autumn, early spring phases again had the strongest reactions. Our important finding, that all spring phases within European countries, except *R. pseudoacacia* flowering, exhibited a stronger response to temperature in

warmer countries with earlier mean onset dates, may allow future parametrization of simple site-specific phenological models where no data were observed.

We would recommend further study to consider some questions arising from this study. Why is responsiveness to temperature greater in warmer countries? Will increased autumn temperatures hinder vernalization and thus delay spring? Will this interfere with spring temperatures advancing spring? To what extent does rainfall and soil moisture influence phenology, particularly of leaf colouration phases? We trust that these, and other questions, can be addressed under COST725 auspices on the European datasets it is assembling.

Our first systematic meta-analysis of more than 100 000 phenological time series in Europe clearly confirmed that there was no reporting or publication bias in earlier studies. There is an evident signal of advancing leaf unfolding, flowering and fruiting in wild plants all across Europe apparent in almost 80% of the records. The mean advance of spring in Europe of 2.5 days decade^{-1} matches previous results for the continent (Menzel & Fabian, 1999) and is slightly above results

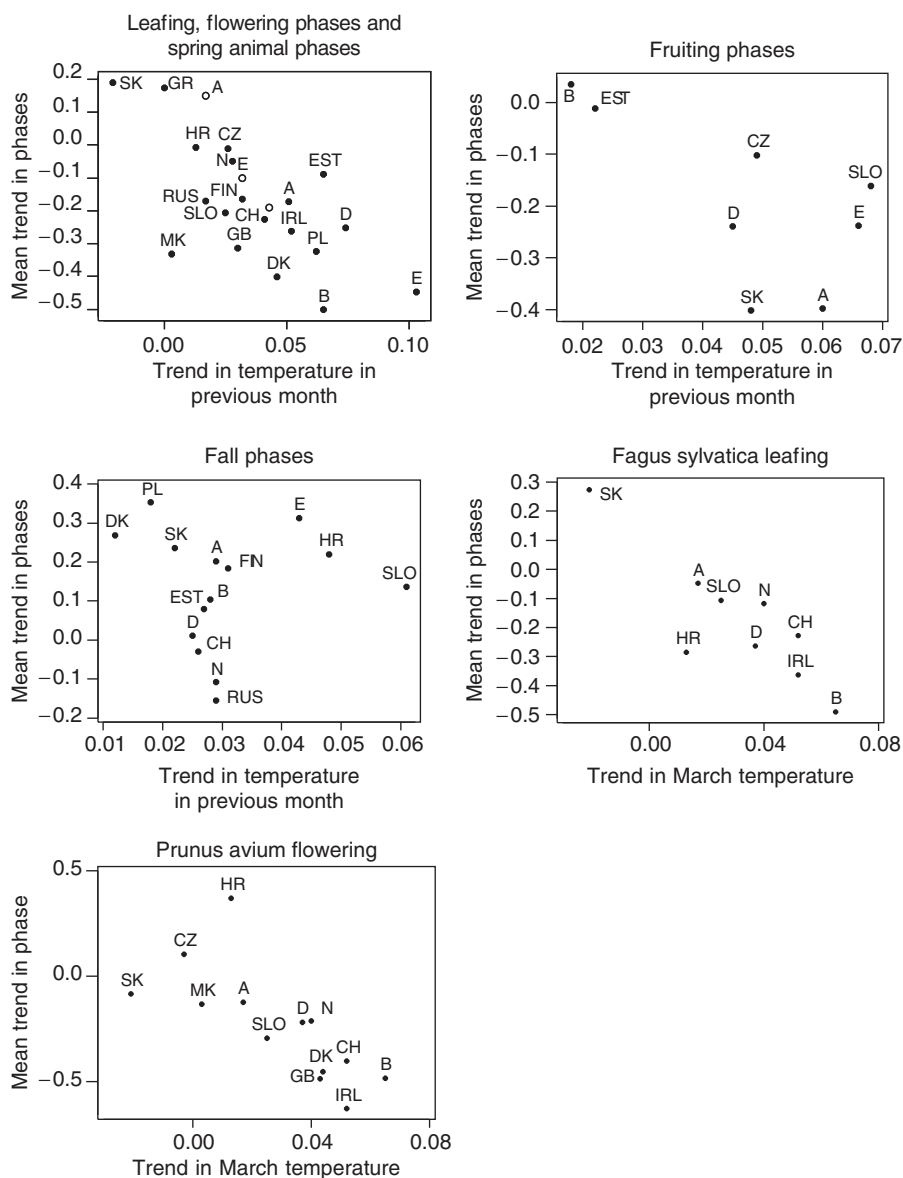


Fig. 4 National mean temperature trends against mean phenological trends. (a) In spring and summer (leaf unfolding, flowering – closed circles, animal phases – open circles). (b) In summer and early autumn (fruit ripening). (c) In autumn (leaf colouring and leaf fall). (d) For leaf unfolding of *Fagus sylvatica* and (e) for flowering of *Prunus avium*. Country abbreviations follow the international country codes.

for a few countries in Central Europe (Defila & Clot, 2001, 2005; Menzel, 2003), however, in accordance with them, as our study period was restricted to the last three decades characterized by a stronger warming trend. Leaf colouring and leaf fall were less frequently observed; the majority of trends analysed were from Germany where, on average, no trend in leaf colouring was found (Fig. 4c; Menzel, 2003). Thus, our summary of all trends revealed no clear signal of leaf colouring changes in the last three decades, whereas results for

other European countries based on fewer records showed delayed autumn (Menzel & Fabian, 1999; Defila & Clot, 2001). Normalized difference vegetation index (NDVI; Myneni *et al.*, 1997; Zhou *et al.*, 2001) and the CO₂ signal (Keeling *et al.*, 1996) provide spatially and species-averaged information on the start and end of the growing season. Confined to shorter time spans starting in 1981 (NDVI), their lengthening of the growing season peak at about 10 days decade⁻¹ for Eurasia (Zhou *et al.*, 2001), probably due to the fact that

ground-based visible colouring or leaf fall occurs later than the end of the growing season derived by NDVI or that the magnitudes derived by NDVI data depends on their coarse temporal resolution. The spring phenological signal, however, is a perfect indicator for climate change impacts, as observed advances quantitatively mirror the measured warming.

Acknowledgements

We thank all anonymous observers in the European national phenological networks for their valuable work and two anonymous referees for the helpful comments. This study was supported by a travel grant from the COST action (A. M.).

References

- Defila C, Clot B (2001) Phytophenological trends in Switzerland. *International Journal of Biometeorology*, **41**, 203–207.
- Defila C, Clot B (2005) Phytophenological trends in the Swiss Alps, 1951–2002. *Meteorologische Zeitschrift*, **14**, 191–196.
- Fitter AH, Fitter RSR (2002) Rapid changes in the flowering time in British plants. *Science*, **296**, 1689–1691.
- Hughes L (2000) Biological consequences of global warming: is the signal already apparent? *Trends in Ecology and Evolution*, **15**, 56–61.
- Keeling CD, Chin JFS, Whorf TP (1996) Increased activity of northern vegetation inferred from atmospheric CO₂ measurements. *Nature*, **382**, 146–149.
- Kozlov MV, Berlina NG (2002) Decline in length of the summer season on the Kola Peninsula, Russia. *Climatic Change*, **54**, 387–398.
- IPCC (2001) Contribution of working group II to the third assessment report of the intergovernmental panel on climate change. In: *Climate Change 2001: Impacts, Adaptations, and Vulnerability* (eds McCarthy JJ, Canziani OF, Leary NA, Dokken DJ, White KS), p. 1032. Cambridge University Press, New York.
- Meier U (1997) *BBCH-Monograph. Growth stages of plants – Entwicklungsstadien von Pflanzen – Estadios de las plantas – Développement des Plantes*. Blackwell Wissenschaftsverlag, Berlin und Wien.
- Menzel A (2002) Phenology: its importance to the global change community. *Climatic Change*, **54**, 379–385.
- Menzel A (2003) Plant phenological anomalies in Germany and their relation to air temperature and NAO. *Climatic Change*, **57**, 243–263.
- Menzel A, Fabian P (1999) Growing season extended in Europe. *Nature*, **397**, 659.
- Mitchell TD, Carter TR, Jones PD *et al.* (2004) *A comprehensive set of high-resolution grids of monthly climate for Europe and the globe: the observed record (1901–2000) and 16 scenarios (2001–2100)*. Tyndall Working Paper 55, July 2004, pp. 1–30.
- Mitchell TD, Hulme M, New M (2002) Climate data for political areas. *Area*, **34**, 109–112.
- Myneni RB, Keeling CD, Tucker CJ *et al.* (1997) Increased plant growth in the northern high latitudes from 1981 to 1991. *Nature*, **386**, 698–702.
- Parmesan C, Yohe G (2003) A globally coherent fingerprint of climate change impacts across natural systems. *Nature*, **421**, 37–42.
- Root TL, Price JT, Hall KR *et al.* (2003) Fingerprints of global warming on wild animals and plants. *Nature*, **421**, 57–60.
- Sparks TH, Menzel A (2002) Observed changes in the seasons: an overview. *International Journal on Climatology*, **22**, 1715–1725.
- Walther GR, Post E, Convey P *et al.* (2002) Ecological responses to recent climate change. *Nature*, **416**, 389–395.
- Zhou LM, Tucker CJ, Kaufmann RK *et al.* (2001) Variations in northern vegetation activity inferred from satellite data of vegetation index during 1981 to 1999. *Journal of Geophysiology Research*, **106**, 20069–20083.



The Impact of Boreal Forest Fire on Climate Warming

J. T. Randerson, *et al.*
Science **314**, 1130 (2006);
DOI: 10.1126/science.1132075

The following resources related to this article are available online at www.sciencemag.org (this information is current as of January 22, 2007):

Updated information and services, including high-resolution figures, can be found in the online version of this article at:

<http://www.sciencemag.org/cgi/content/full/314/5802/1130>

Supporting Online Material can be found at:

<http://www.sciencemag.org/cgi/content/full/314/5802/1130/DC1>

This article **cites 6 articles**, 4 of which can be accessed for free:

<http://www.sciencemag.org/cgi/content/full/314/5802/1130#otherarticles>

This article appears in the following **subject collections**:

Atmospheric Science

<http://www.sciencemag.org/cgi/collection/atmos>

Information about obtaining **reprints** of this article or about obtaining **permission to reproduce this article** in whole or in part can be found at:

<http://www.sciencemag.org/help/about/permissions.dtl>

The Impact of Boreal Forest Fire on Climate Warming

J. T. Randerson,^{1*} H. Liu,² M. G. Flanner,¹ S. D. Chambers,³ Y. Jin,¹ P. G. Hess,⁴ G. Pfister,⁴ M. C. Mack,⁵ K. K. Treseder,¹ L. R. Welp,⁶ F. S. Chapin,⁷ J. W. Harden,⁸ M. L. Goulden,¹ E. Lyons,¹ J. C. Neff⁹ E. A. G. Schuur,⁵ C. S. Zender¹

We report measurements and analysis of a boreal forest fire, integrating the effects of greenhouse gases, aerosols, black carbon deposition on snow and sea ice, and postfire changes in surface albedo. The net effect of all agents was to increase radiative forcing during the first year (34 ± 31 Watts per square meter of burned area), but to decrease radiative forcing when averaged over an 80-year fire cycle (-2.3 ± 2.2 Watts per square meter) because multidecadal increases in surface albedo had a larger impact than fire-emitted greenhouse gases. This result implies that future increases in boreal fire may not accelerate climate warming.

Arctic and boreal regions are warming rapidly, with multiple consequences for northern ecosystems and global climate (1). In boreal ecosystems, future increases in air temperature may lengthen the fire season and increase the probability of fires, leading some to hypothesize a positive feedback between warming, fire activity, carbon loss, and future climate change (2, 3). Although CO₂ and other greenhouse gases emitted by fire contribute to climate warming, understanding the net effect of a changing fire regime on climate is challenging because of the multiple ways by which fires influence atmospheric composition and the land surface. Emissions of aerosols, for example, can lead to either warming or cooling at a regional scale, depending on factors such as aerosol composition and the underlying albedo of both the Earth's surface and clouds (4). Subsequent deposition of black carbon aerosols on glaciers, snow, sea ice, and the Greenland ice sheet may reduce surface albedo (5), causing both atmospheric heating (6) and enhanced surface melting. Within a burn perimeter, combined changes in ecosystem structure and species composition after fire cause net radiation and sensible heat fluxes to decline substantially (7, 8). These changes in the local surface energy budget persist for decades and are probably regionally variable. Concurrently, accumulation of carbon in organic soils and vegetation during intermediate successional stages offsets the pulse of carbon released during combustion (9).

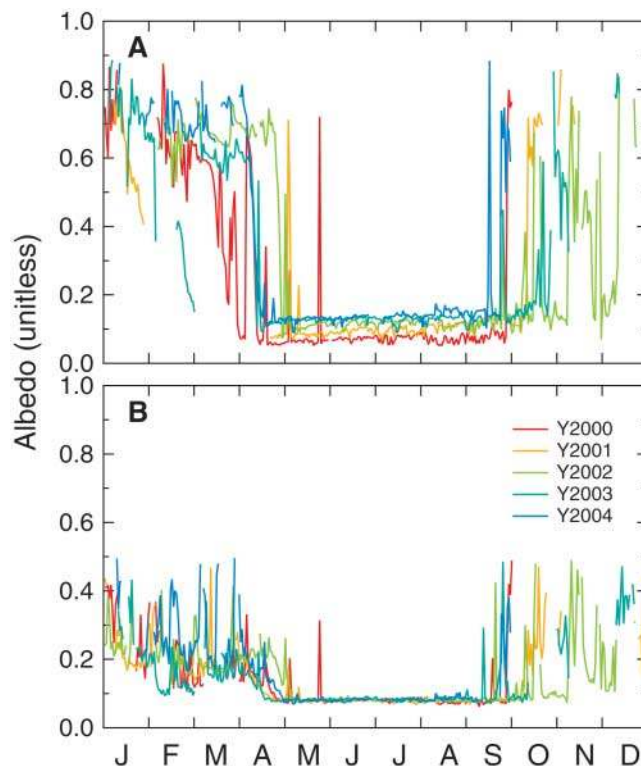
Understanding the net effect of these processes (and their temporal and spatial scales) is important in managing northern forests to mitigate the climate impacts of fossil fuel emissions. Although changes in boreal forest albedo can have a considerable cooling effect on Northern Hemisphere climate (10, 11), these changes are offset by accompanying changes in carbon accumulation (12), so the net effect of land cover change on climate may be close to neutral at a global scale when both surface energy balance and CO₂ fluxes are considered (13). Here we applied the concept of radiative forcing (12) to assess quantitatively the net effect of a boreal forest fire on climate, on the basis of carbon and surface energy budget measurements that we made in a fire chronosequence of black spruce (*Picea mariana*) in interior Alaska. We considered two time scales: the year immediately after fire and an 80-year period

during which species composition and ecosystem structure returned to a prefire mature successional state as defined by an adjacent unburned control stand.

The Donnelly Flats crown fire occurred during 11 to 18 June 1999 in interior Alaska (63°55'N; 145°44'W) and burned ~7600 ha (14). The fire was intense (e.g., figs. S1 and S2), causing stand-replacing mortality of the black spruce within the burn perimeter and consuming much of the soil organic matter above the mineral horizon (15). Aboveground fuel consumption from overstory and understory vegetation was estimated with a combination of harvesting, allometry, and inventory methods. Postfire soil respiration losses during the first year after fire were estimated with a combination of chamber measurements and eddy covariance measurements. Precision spectral pyranometers (Eppley Laboratory, Inc., Newport, RI) measured incoming and outgoing shortwave radiation above the canopy (and thus surface albedo) during July and August of 1999 within the burn perimeter (7) and then mostly continuously from October 1999 through September 2004 at both the burn and control.

We converted field measurements of carbon loss during the fire to CH₄ and CO₂ fluxes using emission factors (16). Radiative forcing from these greenhouse gases was estimated with equations derived from a global radiative transfer model (17). In our figures and table, we report global annual mean radiative forcing (in W) per m² of burned area, with radiative forcing defined following the Intergovernmental Panel on Climate Change Third Assessment Report convention as the change in net radiation at the tropopause after stratospheric ad-

Fig. 1. Midday surface albedo within the burn perimeter of the Donnelly Flats fire (A) and from the adjacent black spruce stand that served as a control (B). Summer albedo progressively increased during each year and exceeded values at the control site ~3 years after fire. Snow events, including one in late May of 2000, caused spikes that are visible at both the burn and control sites.



¹Department of Earth System Science, University of California, Irvine, CA 92697, USA. ²Department of Physics, Atmospheric Science, and General Science, Jackson State University, Jackson, MS 39217, USA. ³Australian Nuclear Science and Technology Organization, Environmental Division, Menai, NSW 2234, Australia. ⁴Atmospheric Chemistry Division, National Center for Atmospheric Research, Boulder, CO 80301, USA. ⁵Department of Botany, University of Florida, Gainesville, FL 32611, USA. ⁶Environmental Science and Engineering, California Institute of Technology, Pasadena, CA 91125, USA. ⁷Institute of Arctic Biology, University of Alaska, Fairbanks, AK 99775, USA. ⁸U.S. Geological Survey, Menlo Park, CA 94025, USA. ⁹Geological Sciences and Environmental Studies, University of Colorado at Boulder, Boulder, CO 80309, USA.

*To whom correspondence should be addressed. E-mail: jranders@uci.edu

justment (18). CH₄ was assumed to have a 10-year atmospheric lifetime. The lifetime of the CO₂ anomaly from the fire was estimated with a combination of ocean impulse-response functions from the Joos and Siegenthaler ocean carbon model (19) and a postfire trajectory of net ecosystem production (NEP) that we constructed using mass balance constraints and eddy covariance measurements (figs. S3 and S4). We used the Column Radiation Model (20) to estimate radiative forcing from changes in surface albedo within the Donnelly Flats burn perimeter (figs. S5 to S8). The persistence of albedo changes in postfire ecosystems was assessed from an analysis of Moderate Resolution Imaging Spectroradiometer (MODIS) albedo measurements (21) within burn perimeters of known ages (14) across interior Alaska. We derived radiative forcing from the fire-induced ozone anomaly using simulations from the National Center for Atmospheric Research Community Atmosphere Model version 3 (CAM 3) of the 2004 Alaska and Yukon fire complex (22) scaled to the carbon emission levels that we measured for the Donnelly Flats fire. Similarly, we estimated radiative forcing from the direct effect of aerosols and deposition of black carbon on snow and sea ice by injecting emissions from the Donnelly Flats fire into CAM 3 (23, 24). In the Supporting Online Material we provide more information about our methods for estimating radiative forcing, as well as an additional set of forcing estimates that take into account the efficacy of the different agents (25).

During the fire event, $206 \pm 110 \text{ g C m}^{-2}$ were emitted by combustion from the black spruce overstory, $107 \pm 74 \text{ g C m}^{-2}$ from the vascular plant understorey, and $1246 \pm 600 \text{ g C m}^{-2}$ from the duff layer composed of mosses, lichens, roots, partially decomposed plant litter, and humus. Total fuel consumption for the Donnelly Flats fire ($1560 \pm 610 \text{ g C m}^{-2}$) was similar to other estimates for boreal North America, including 1580 g C m^{-2} for moderately severe fires in boreal North America (26) and 1300 g C m^{-2} for the mean of Canadian boreal forests (27). Including additional soil respiration losses of $202 \pm 53 \text{ g C m}^{-2} \text{ year}^{-1}$ during the first year after fire, the ecosystem lost a total of $1760 \pm 620 \text{ g C m}^{-2}$.

Radiative forcing from long-lived greenhouse gases (CH₄ and CO₂) contributed a total of $8 \pm 3 \text{ W m}^{-2}$ during the first year. Deposition of black carbon on snow and sea ice added another $8 \pm 5 \text{ W m}^{-2}$. An increase in tropospheric ozone from fire-emitted trace gases generated a positive radiative forcing of $6 \pm 4 \text{ W m}^{-2}$. Fire-emitted aerosols mixed widely across arctic and boreal regions (fig. S9), decreased net radiation at the surface ($-90 \pm 35 \text{ W m}^{-2}$), but did not substantially change radiative forcing ($17 \pm 30 \text{ W m}^{-2}$). Changes in surface albedo within the fire perimeter offset positive radiative forcing from the other agents. Specifically, the loss of overstorey canopy after fire led to increased snow exposure during spring and fall (fig. S10), higher albedo (Fig. 1), and a negative annual radiative forcing

($-5 \pm 2 \text{ W m}^{-2}$). The combined effect of all forcing agents was $34 \pm 31 \text{ W m}^{-2}$ during year 1 (Table 1).

After the first year, the short-lived effects of ozone, aerosols, and black carbon deposition were no longer important, so the net effect of the fire on radiative forcing reflected the balance between the persistence of postfire changes in surface albedo and the effects from the remaining greenhouse gases in the atmosphere. During the first 5 years after fire, summer albedo progressively increased (Fig. 1), probably from an increase in grass and shrub cover and partial loss of black carbon that initially coated soil surfaces and dead black spruce boles. This strengthened the negative radiative forcing

from postfire albedo changes, with this quantity decreasing from $-5 \pm 2 \text{ W m}^{-2}$ during the first year to $-8 \pm 3 \text{ W m}^{-2}$ during the period 3 to 5 years after fire. Analysis of MODIS satellite data from nearby forest stands provided evidence that spring and summer albedo typically remains elevated for about three decades after fire and that recovery to prefire albedo levels requires ~ 55 years (Fig. 2).

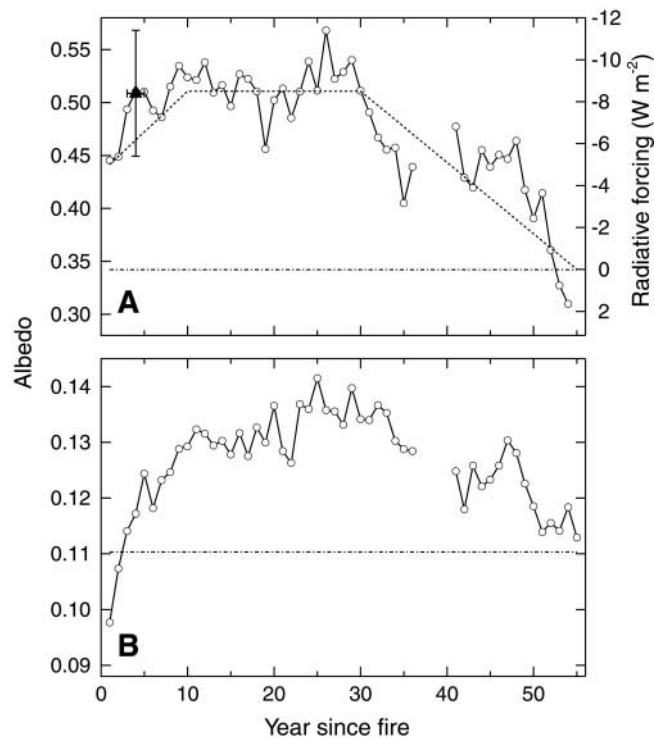
We predicted that the greenhouse gas pulse from the Donnelly Flats fire should gradually decline over a period of 5 decades, owing to CH₄ oxidation and CO₂ uptake by the oceans and regrowing vegetation within the burn perimeter (fig. S3D). During this interval, the greenhouse gases will contribute to a positive radiative forcing

Table 1. Radiative forcing associated with the Donnelly Flats fire.

Forcing agent	Radiative forcing* [W (m ² burned) ⁻¹]	
	Year 1	Years 0 to 80 (mean)
Long-lived greenhouse gases (CH ₄ and CO ₂)	8 ± 3	1.6 ± 0.8
Ozone	6 ± 4	0.1 ± 0.1
Black carbon deposition on snow	3 ± 3	0.0 ± 0.0
Black carbon deposition on sea ice	5 ± 4	0.1 ± 0.1
Aerosols (direct radiative forcing)†	17 ± 30	0.2 ± 0.4
Impact at the surface: $-90 \text{ W} \pm 35 \text{ m}^{-2}$		
Changes in post-fire surface albedo	-5 ± 2	-4.2 ± 2.0
Total‡	34 ± 31	-2.3 ± 2.2

*All the radiative forcing estimates reported here represent annual mean values (in W) for the global atmosphere associated with burning of a 1-m² area within the perimeter of the Donnelly Flats fire. We report values averaged over year 1 and for the mean of the 0- to 80-year period after fire (and including the fire event). †We did not estimate indirect effects of aerosols on radiative forcing as mediated, for example, by cloud drop sizes or cloud lifetime (4). Although uncertain, indirect aerosol effects are thought to contribute to negative radiative forcing (18, 25) and would offset other positive radiative forcing agents during year 1. ‡Accounting for the efficacy of the different forcing agents (25), the total effective forcing of the Donnelly Flats fire was $18 \pm 42 \text{ W m}^{-2}$ during year 1 and $-2.4 \pm 2.3 \text{ W m}^{-2}$ during years 0 to 80 (tables S1 and S2).

Fig. 2. Postfire albedo during (A) spring (Julian Days 33 to 113) and (B) summer (Julian Days 145 to 241) from MODIS satellite observations extracted from burn scars of different ages in interior Alaska (circles and solid line, left axis). A control was constructed from the mean of evergreen conifer vegetation that did not burn in the last 55 years (dashed-dotted line, left axis). Annual radiative forcing as estimated from tower measurements of albedo from burn and control sites during 2002 to 2004 was $-8 \pm 3 \text{ W m}^{-2}$ [(A), triangle, right axis]. The longer-term postfire trajectory of albedo-driven annual radiative forcing was assumed to follow the MODIS albedo pattern [(A), triangle, right axis]. Years with limited burned area were excluded from the analysis.



(Fig. 3A). After ~60 years, continued uptake by the postfire ecosystem should cause atmospheric CO₂ to decrease below background levels, subsequent withdrawal of CO₂ from the ocean, and a negative radiative forcing. As a result of this trajectory and concurrent changes in surface albedo, the influence of the fire on radiative forcing depends on the averaging period (Fig. 3B). Averaged over years 0 to 80, net radiative forcing from the different forcing agents was $-2.3 \pm 2.2 \text{ W m}^{-2}$ (Table 1).

A change in fire return times will have consequences for climate forcing (Fig. 3C), based on the time-since-fire trajectories of the different forcing agents estimated from the Donnelly Flats fire, combined with a stand age model (28). If the fire return time decreases [as has been suggested from future warming and drying in continental interiors (29)], loss of carbon will increase radiative forcing (Fig. 3C). Accounting for all

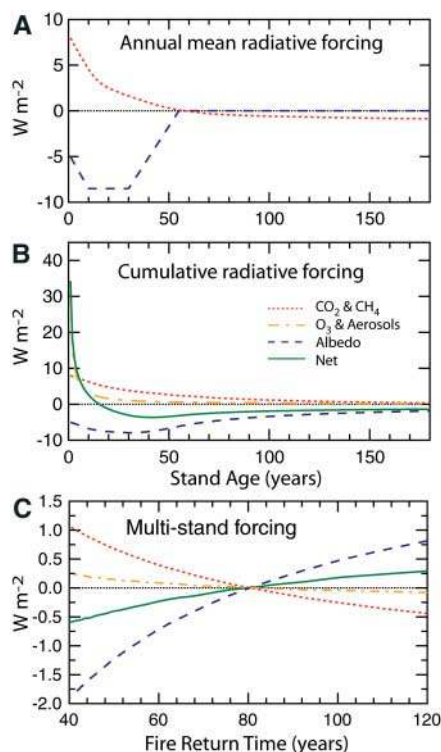


Fig. 3. (A) Annual radiative forcing from long-lived greenhouse gases and the postfire trajectory of surface albedo. (B) Cumulative annual radiative forcing for the different forcing agents averaged over the time since the fire (or equivalently, the age of the stand). (C) Climate forcing of the different components as a function of the fire return time relative to a distribution of stands at steady state with a mean fire return time of 80 years. (C) was constructed with postfire trajectories for the individual agents measured or predicted for the Donnelly Flats fire [e.g., (A)] and the forest stand age distribution model described in the Supporting Online Material. For (C), by definition, each forcing agent had a zero mean at steady state (at a mean fire return time of 80 years).

forcing agents, however, leads to a small negative radiative forcing at the global scale (Fig. 3C) and calls into question the positive feedback that has been suggested in past work. The cooling from a decrease in fire return times is likely to be substantially larger in the Northern Hemisphere, taking into account the spatial pattern of the temperature anomalies resulting from the different forcing agents. Specifically, radiative forcing from greenhouse gases has a widely distributed impact on global temperature (18), whereas the influence of postfire changes in surface albedo will be concentrated almost entirely in northern regions (10, 11, 13, 18).

For the boreal biome as a whole, key factors that are likely to determine the balance between negative and positive radiative forcing associated with fire include burn severity, species establishment in postfire ecosystems, and the duration of winter snow cover. Increased burn severity, for example, may increase aerosol and greenhouse gas emissions, but it is not clear to what extent this may be canceled by greater loss of canopy overstory and consequently higher albedo values during winter and spring. Another unresolved question involves the extent to which fire in Siberian larch forests, which are needle-leaf deciduous, has the same influence on post-fire surface albedo as reported here for North American needleleaf evergreen forests. Decreases in spring snow cover (30) may weaken negative feedbacks associated with postfire increases in surface albedo documented in North America.

Future interactions between the land surface and climate in northern regions may involve both negative feedbacks within the boreal interior (via mechanisms outlined here) and positive feedbacks involving shrub and forest expansion in arctic tundra ecosystems (31) and loss of snow cover. Our analysis illustrates how ecosystem processes that generate carbon sources and sinks have inseparable consequences for other forcing agents (12, 13, 32, 33). To the extent that the contemporary Northern Hemisphere carbon sink originates from changes in northern forest cover and age (34), its value from a climate perspective requires a more nuanced view that encompasses all agents of radiative forcing. Important next steps include reducing uncertainties associated with direct and indirect aerosol effects and disturbance-linked changes in albedo, exploring the combined impacts of feedbacks of the forcing agents estimated here within climate models, and extending this approach to assess the radiative forcing associated with land-cover transitions in temperate and tropical ecosystems.

References and Notes

- ACIA, "Arctic Climate Impact Assessment" (Cambridge Univ. Press, Cambridge, UK, 2005).
- W. A. Kurz, M. J. Apps, B. J. Stocks, W. J. A. Volney, in *Biotic Feedbacks in the Global Climate System: Will the Warming Speed the Warming?* G. M. Woodwell,

- F. Mackenzie, Eds. (Oxford Univ. Press, Oxford, UK, 1995), pp. 119–133.
- E. S. Kasischke, B. J. Stocks, *Fire, Climate Change, and Carbon Cycling in the Boreal Forest*. M. M. Cadwell et al., Eds., Ecological Studies (Springer, New York, 2000).
- V. Ramanathan, P. J. Crutzen, J. T. Kiehl, D. Rosenfeld, *Science* **294**, 2119 (2001).
- S. G. Warren, W. J. Wiscombe, *J. Atmos. Sci.* **37**, 2734 (1980).
- J. Hansen, L. Nazarenko, *Proc. Natl. Acad. Sci. U.S.A.* **101**, 423 (2004).
- S. D. Chambers, F. S. Chapin, *J. Geophys. Res.* **108**, 8145 (2002).
- H. Liu, J. T. Randerson, J. Lindfors, F. S. Chapin, *J. Geophys. Res.* **110**, D13101 (2005).
- J. W. Harden et al., *Global Change Biol.* **6**, 174 (2000).
- G. B. Bonan, D. Pollard, S. L. Thompson, *Nature* **359**, 716 (1992).
- P. K. Snyder, C. Delire, J. A. Foley, *Clim. Dyn.* **23**, 279 (2004).
- R. A. Betts, *Nature* **408**, 187 (2000).
- V. Brovkin et al., *Global Change Biol.* **10**, 1253 (2004).
- The Alaska Fire Service maintains a database of annual fire statistics and geographic information system (GIS) burn perimeters (<http://agdc.usgs.gov/data/blm/fire/>).
- J. C. Neff, J. W. Harden, G. Gleixner, *Can. J. For. Res. Rev. Can. Rech. For.* **35**, 2178 (2005).
- M. O. Andreae, P. Merlet, *Global Biogeochem. Cycles* **15**, 955 (2001).
- G. Myhre, E. J. Highwood, K. P. Shine, F. Stordal, *Geophys. Res. Lett.* **25**, 2715 (1998).
- V. Ramaswamy et al., in *Climate Change 2001: The Scientific Basis. Contributions of Working Group 1 to the Third Assessment Report of the Intergovernmental Panel on Climate Change*, J. T. Houghton et al., Eds. (Cambridge Univ. Press, Cambridge, UK, 2001), pp. 350–416.
- I. G. Enting, T. M. L. Wigley, M. Heimann, "Future Emissions and Concentrations of Carbon Dioxide: Key Ocean/Atmosphere/Land Analyses" (Technical paper no. 31, Commonwealth Scientific and Industrial Research Organization Division of Atmospheric Research, 2001).
- B. P. Briegleb, *J. Geophys. Res.* **97**, 7603 (1992).
- C. B. Schaaf et al., *Remote Sens. Environ.* **83**, 135 (2002).
- G. Pfister et al., *Geophys. Res. Lett.* **32**, L11809 (2005).
- P. J. Rasch, W. D. Collins, B. E. Eaton, *J. Geophys. Res.* **106**, 7337 (2001).
- M. G. Flanner, C. S. Zender, *J. Geophys. Res.* **111**, D12208 (2006).
- J. Hansen et al., *J. Geophys. Res.* **110**, D18104 (2005).
- E. S. Kasischke et al., *Global Biogeochem. Cycles* **19**, GB1012 (2005).
- B. D. Amiro et al., *Can. J. For. Res. Rev. Can. Rech. For.* **31**, 512 (2001).
- E. A. Johnson, *Fire and Vegetation Dynamics: Studies from the North American Boreal Forest*, H. J. B. Birks, Ed., Cambridge Studies in Ecology (Cambridge Univ. Press, Cambridge, UK, 1992).
- M. D. Flannigan, K. A. Logan, B. D. Amiro, W. R. Skinner, B. J. Stocks, *Clim. Change* **72**, 1 (2005).
- Z. M. Kuang, Y. L. Yung, *Geophys. Res. Lett.* **27**, 1299 (2000).
- F. S. Chapin et al., *Science* **310**, 657 (2005).
- G. P. Robertson, E. A. Paul, R. R. Harwood, *Science* **289**, 1922 (2000).
- R. A. Pielke et al., *Philos. Trans. R. Soc. London Ser. A* **360**, 1705 (2002).
- C. L. Goodale et al., *Ecol. Appl.* **12**, 891 (2002).
- This work was supported by NSF and NASA grants (OPP-0097439 and NNG04GK49G, respectively). We thank M. Prather for advice and C. Dunn, J. Henkelman, J. Raymond, and J. Garron for technical assistance.

Supporting Online Material

www.sciencemag.org/cgi/content/full/314/5802/1130/DC1
Materials and Methods

SOM Text

Figs. S1 to S10

Tables S1 and S2

References and Notes

5 July 2006; accepted 3 October 2006

10.1126/science.1132075



Supporting Online Material for

The Impact of Boreal Forest Fire on Climate Warming

J. T. Randerson,* H. Liu, M. G. Flanner, S. D. Chambers, Y. Jin, P. G. Hess, G. Pfister,
M. C. Mack, K. K. Treseder, L. R. Welp, F. S. Chapin, J. W. Harden, M. L. Goulden, E.
Lyons, J. C. Neff, E. A. G. Schuur, C. S. Zender

*To whom correspondence should be addressed. E-mail: jranders@uci.edu

Published 17 November 2006, *Science* **314**, 1130 (2006)
DOI: 10.1126/science.1132075

This PDF file includes:

Materials and Methods
SOM Text
Figs. S1 to S10
Tables S1 and S2
References and Notes

Supporting Online Material

Materials and Methods

SOM Text

Figs. S1-S10

Tables S1 and S2

References and notes

1. Supporting materials and methods

Overview

Here we present details of the approaches we used to quantify the different forcing agents associated with the Donnelly Flats fire, which burned during 11-18 June 1999 in interior Alaska (63° 55' N; 145° 44' W) as a result of human ignition. As described in the main text, we developed radiative forcing estimates for the first year immediately after fire and over a period of 80 years after fire (including the first year). The longer interval represented the amount of time required for the vegetation to recover to a pre-fire state that was defined by our control stand. This fire was so small that it had a minor effect on the global radiation budget. Nevertheless, working out the contribution of the various forcing agents and their combined effect for a single fire is a necessary step towards assessing the impact of a changing boreal fire regime on climate at regional or continental scales.

Radiative forcing: Definition and Units

In the main text and supporting online material, we consider the influence of 1 m² of burned area from the Donnelly Flats fire. We consider the fire emissions from this 1 m² in terms of their influence on global annual mean radiative forcing from long-lived greenhouse gases, tropospheric O₃, the direct effect of atmospheric aerosols, and deposition of black carbon on remote snow and ice. We also estimate radiative forcing from post-fire changes in surface albedo within the burn perimeter. We follow the Intergovernmental Panel on Climate Change (IPCC) Third Assessment Report (TAR) definition of radiative forcing. Specifically, radiative forcing is defined as the change in net radiation at the tropopause caused by the forcing agent, after the stratosphere adjusts radiatively to the agent (*I*).

We report global annual mean radiative forcing (in W) per m² of burned area. By 'global' we mean, for example, that we considered the perturbation to the Earth's total radiation budget from CO₂ pulse released by the fire mixing uniformly throughout the atmosphere. Similarly, for the aerosol and ozone forcings, the mixing pattern was non-uniform, and so we summed the perturbation from the fire to the radiation budget across the Earth's entire surface (across all of the atmospheric model grid cells). As described above, the radiative forcing estimates in Table 1 and throughout the main text include stratospheric adjustment, and so to compare directly with Intergovernmental Panel on Climate Change Third Assessment Report estimates (*I*) they should be divided by the area of the earth. More detailed information about our approach for estimating radiative

forcing is provided in section 1.11. In several cases we had to convert from instantaneous forcing at the tropopause to adjusted forcing (the IPCC standard) using published estimates of how these two quantities are related (2, 3).

1.1 Estimating carbon emissions from the Donnelly Flats fire

We used a combination of standard inventory and allometric methods (4) with a survey of burn severity to estimate biomass and carbon of trees greater than 1.37 m in height consumed in the 1999 Donnelly Flats fire. Within the eddy covariance tower footprint, 16 plots (100 m² each) were established in four blocks (n = 4) with greater than 100 m between blocks. The diameter at breast height (DBH; 1.37 m) was measured and burn severity was estimated for all trees (standing and fallen) in these plots. Burn severity was assigned a percent score for each of the following classes: needles consumed, fine branches consumed, coarse branches consumed, cones consumed, and bark consumed. Site-specific allometric equations based on DBH (M.C. Mack, unpublished data) were then used to calculate pre-fire biomass pools for each tree. Biomass pools were assumed to consist of 50% carbon. Carbon lost per tree was calculated as the sum of pre-fire pools multiplied by the fraction of the pool consumed during the fire. Trees were summed within plots, and divided by 100 m² to yield C loss per m². Biomass loss from the vascular plant understory was calculated as the difference between the mean of post-fire aboveground understory biomass (immediately following the fire) in ten 1 m² plots randomly distributed in the tower footprint of the burn site and the mean understory biomass in the control site tower footprint.

Total carbon loss from surface soils, non-vascular plants, and lichens during the Donnelly Flats fire was estimated in two ways by Neff et al. (5). The first involved directly measuring the change in total soil organic matter (SOM) between 8 control plots and 6 burn plots. A second approach involved using Al (a non-volatile element conserved during the fire) to estimate the fuel loads and loss within individual burned plots, via a comparison with the Al to C ratio of SOM in the control plots. Carbon transferred from aboveground vegetation to the soil during and immediately after fire is accounted for in these soil measurements. These two approaches yielded slightly different estimates: 1071 ± 537 g C m⁻² and 1421 ± 267 g C m⁻², respectively. Here we used the average of these two approaches 1246 ± 600 g C m⁻².

1.2 Estimating additional carbon losses during the first year after fire

We estimated additional soil respiration carbon losses during year 1 using a combination of chamber, eddy covariance, and modeling approaches. Chamber measurements of soil respiration were made at six sites within the eddy covariance tower footprint four times a day, for a total of eight days between the 5th and 26th of July 1999. A LI-COR 6200 portable photosynthesis system was used in conjunction with a 20 cm diameter (8 L Plexiglas) chamber within which the air was circulated using a pair of slow moving 50 mm fans (6). The chamber was allowed to equilibrate to ambient pressure via a 20 cm length of 1 mm inner diameter copper tubing mounted through the top of the chamber. Each measurement consisted of ten CO₂ concentration observations at eight-second intervals. A regression of CO₂ with time was then performed from which respiration estimates were made based on chamber temperature, humidity, and ambient pressure. For each measurement the chamber was clamped to pre-installed PVC collars that were each left in position for the duration of the measurement period. The collars

were each cut at least 10 cm into the charred surface using a sharpened soil corer so that they were firmly seated in mineral soil. The mean and standard error of the chamber observations during July was $1.5 \pm 0.2 \mu\text{mol m}^{-2} \text{s}^{-1}$.

We used a combination of 3-D ultrasonic anemometer (Solent 1199HSH, Gill Instruments Ltd., England) and closed-path, infrared-absorption $\text{H}_2\text{O}/\text{CO}_2$ gas analyzer (IRGA: LI-6262, LI-COR Inc., Lincoln, NB, U.S.A.) to make flux measurements within the Donnelly Flats burn scar during July 1999 and during March – June of 2000. We mounted the sonic anemometer and IRGA intake on a 3 m boom, at a height of 5.1 m, on a 15 m aluminum tower (Climatronics Corp., Bohemia, NY, U.S.A.). Since the longest and most homogeneous fetch regions of the burn scar extended north, east and south of the measurement site, and prevailing winds were usually oriented north-south, we oriented the mounting boom approximately east/northeast.

The IRGA was aspirated at approximately $8 \text{ liters min}^{-1}$ using a diaphragm pump (UN815-KTDC, KNF Neuberger, Trenton, NJ, U.S.A.) via a 3.3 mm internal diameter "Bev-a-Line" intake tube (Thermoplastic Processes Inc., Sterling, NJ, U.S.A.). This flow rate was sufficient to rapidly flush the IRGA's optical bench as well as maintain turbulent flow in the sampling line, important requirements for performing eddy-covariance flux measurements with a closed-path analyzer. We installed a 1.3 liter PVC buffer volume between the diaphragm pump and the IRGA to reduce pressure pulsing effects. We constructed the initial 1.5 m of the IRGA's intake line from insulated copper tubing to minimize temperature-induced density fluctuations in the sample air stream (7).

We performed two-point (zero and span) calibrations on the IRGA for water vapor and CO_2 at regular intervals. The zero calibration was performed using ultra-high purity nitrogen. Span checks for water vapor and CO_2 were performed using a precision dew-point generator (LI-610, LI-COR Inc.) and a balanced CO_2 standard, respectively. Prior to calculating the turbulent fluxes we performed a coordinate rotation of the wind vector such that the u component was inline with the sonic axis (8). To account for slight variations in sample flow rate due to varying pump performance and ambient wind conditions, we calculated, and corrected for, the lag time between the sonic anemometer and IRGA signals for each 30-minute block of data. Under conditions when the lag time was poorly defined (typically near neutral stability), we adopted the daily modal lag time. We linearly detrended each 30-minute data block to remove contributions from scales of turbulence too large to be sampled within that time period. We made the final flux estimates by taking 30-minute averages over the diurnal cycle.

With closed path IRGAs in particular, there are several factors that contribute independently to underestimated flux estimates, including: the distance between instruments, instrument response time and signal attenuation (9). We adopted an approach that involved the calculation of an "induction factor" to account for the discrepancy between the observed and an idealized cospectrum as a result of the collective system inadequacies (10). The induction factor is unique to a given instrumental setup and, once determined, can be applied to the whole measurement period. The factor with which we eventually corrected the covariance estimates was determined separately for each 30-minute block as a function of the induction factor, measurement height, wind speed and atmospheric stability (equations 32 and 33 in (10) for unstable and stable conditions, respectively). All post processing was performed using a FORTRAN time series analysis package called 'RAMF' version 8.1 (11). Eddy flux measurements during July of 1999 during the same times as the chamber measurements yielded a net flux of $1.8 \pm 0.3 \mu\text{mol m}^{-2} \text{s}^{-1}$. We averaged the eddy covariance and

chamber estimates of CO₂ flux from July to obtain a flux estimate of $1.7 \pm 0.3 \mu\text{mol m}^{-2} \text{s}^{-1}$.

From eddy covariance measurements made during the following spring, we obtained flux estimates of 0.46 ± 0.41 , 0.49 ± 0.49 , and $0.49 \pm 0.53 \mu\text{mol m}^{-2} \text{s}^{-1}$ for April, May, and the first part of June. For the period in between these two measurement periods (August-March), we constructed a simple temperature-dependent model with a Q₁₀ of 2 based on monthly mean surface air temperatures. We adjusted the baseline soil respiration rate such that the model and measured fluxes optimally matched both the July and the following May flux data. For the modeled fluxes we assumed an error of $\pm 50\%$ reflecting uncertainties in our understanding of the temperature sensitivity of respiration and winter controls on microbial processes. The sum of modeled losses over this interval was $99 \pm 49 \text{ g C m}^{-2}$. The total ecosystem respiratory loss during the first post-fire year was $202 \pm 53 \text{ g C m}^{-2} \text{ yr}^{-1}$.

1.3 Post-fire net ecosystem production (NEP) trajectory

To construct a trajectory of post-fire carbon accumulation (fig. S3A), we used three constraints. The first was that after 80 years (the approximate age of the adjacent control stand) the ecosystem accumulated as much carbon as was lost during the first year of the fire (fig. S3B). This constraint ensured consistency with the observations from the control site that were used to estimate the pre-fire duff layer thickness and the allometry relationships used to estimate the loss of aboveground biomass.

Second, we assumed that the annual rate of carbon accumulation was greatest during a deciduous phase from 10 to 40 years. The basis for this constraint was a series of eddy covariance CO₂ flux measurements that we made during 2002-2004 within the perimeter of the Donnelly Flats fire, in a stand that burned in 1987, and in the control. The eddy covariance system used during this latter period consisted of a CSAT3 sonic anemometer (Campbell Sci Ltd., Logan, UT, USA) and LiCor 7500 CO₂/H₂O IRGA (LICOR Inc., Lincoln, NB, USA). Details of the eddy covariance calculations are provided in Liu et al. (12) and Welp et al. (13). Integrated carbon uptake during the growing season (May-September), was $-31 \pm 20 \text{ g C m}^{-2}$ at the Donnelly Flats fire, $-191 \pm 33 \text{ g C m}^{-2}$ at the Granite Creek fire that burned in 1987, and $-152 \pm 9 \text{ g C m}^{-2}$ at the control stand averaged over 2002-2004 (and with standard deviations reflecting interannual variability in fluxes). Growing season net CO₂ uptake was greatest in the deciduous forest (fig S4) and provides partial evidence for high rates of C accumulation during intermediate stages of succession. These eddy covariance measurements from the fire chronosequence also provide some evidence that the transition from a net source in the first year after fire to a net sink occurs within the first decade. This result is consistent with the moderate to severe burn severity observed within the perimeter of the Donnelly Flats fire (5); much of the soil organic C pool was consumed during the fire, leaving a relatively small pool available for decomposition.

A third constraint was that after 40 years (the end of the deciduous phase), the rate of C accumulation slowed following an exponential function and with a relaxation time of 75 years. This ensured that after 150 years, the carbon balance of the forest was close to steady state, and consistent with observations from other older black spruce stands (14). A slowing of the carbon accumulation rate of this magnitude is also consistent with first-order decomposition and accumulation rate constants derived from radiocarbon

measurements in other boreal forest stands with feathermoss ground cover (15). Trumbore and Harden (15) predicted accumulation rates of approximately $12 \pm 13 \text{ g C m}^{-2} \text{ yr}^{-1}$ and $4 \pm 2 \text{ g C m}^{-2} \text{ yr}^{-1}$ for feathermoss and sphagnum cover, respectively for an approximately 150 year old black spruce (OBS) site in Canada. With the NEP curve shown in fig. S3A, we estimate NEP to be $7 \text{ g C m}^{-2} \text{ yr}^{-1}$ at 150 years after fire. We recognize that our accumulation rates are lower than other reported trajectories in the boreal forest (16, 17) and attribute this to the well-drained soils and lack of permafrost at our sites that probably slowed rates of both vegetation and soil carbon accumulation. We assumed that other carbon gain/loss pathways, including leaching and organic C losses were negligible so that NEP was equal to net ecosystem carbon balance (NECB) (18).

1.4 Estimating the radiative forcing from fire emissions of CO₂ and CH₄

We used the total carbon emissions estimates described in section 1.1 along with emissions factors (19) and the assumption that 0.50 g C corresponds to 1 g biomass to estimate fluxes of CO₂ and CH₄ from the fire. We assumed that these trace gases were instantly well mixed in the global atmosphere, that all CO was oxidized to CO₂, and that for the first year, all of the CO₂ and CH₄ emitted by the fire remained airborne. We also considered the indirect production of CH₄ via temporary suppression of atmospheric OH levels by fire-emitted CO (20-22). We assumed that 100 molecules of fire-emitted CO was equivalent to 8 additional molecules of CH₄ (21). Radiative forcing from CO₂ and CH₄ was estimated using equations (and updated constants) from Table 3 of Myhre et al. (23). Radiative forcing from CO₂ and CH₄ during year 1 was $8.0 \pm 3.3 \text{ W m}^{-2}$, with $6.0 \pm 2.1 \text{ W m}^{-2}$ from CO₂, $1.0 \pm 0.4 \text{ W m}^{-2}$ from direct CH₄ emissions, and $1.0 \pm 0.6 \text{ W m}^{-2}$ from indirect effects of CO on the background CH₄ reservoir. Our error estimate includes a component from emissions ($\pm 2.8 \text{ W m}^{-2}$) and a component associated with our subjective assessment of the uncertainty associated with the radiative transfer model ($\pm 0.5 \text{ W m}^{-2}$).

After the first year, we allowed the fire-emitted CH₄ (and its influence on radiative forcing) to decrease with an atmospheric lifetime of 10 years, reflecting oxidation by OH and other sink processes. Fire-emitted CO₂ was removed from the atmosphere by two sinks: the accumulation of carbon in the recovering post-fire ecosystem and via ocean exchange. In considering this single fire, we assumed the rest of the terrestrial biosphere was neither a sink nor a source. Our approach for estimating the post-fire trajectory of net ecosystem production (NEP) and subsequent carbon accumulation is described in section 1.3. Ocean uptake of the fire-emitted CO₂ pulse was estimated using an impulse response function from the Joos and Siegenthaler ocean carbon model as described by Enting et al. (2001). This response function (fig. S3C) was constructed assuming that the emitted pulse occurred at contemporary CO₂ levels and that fossil fuel emissions continue on a trajectory required for stabilization of atmospheric CO₂ at 650 ppm by 2100 (24). In each year after fire, ocean exchange acted only upon the component of the fire-emitted CO₂ pulse that remained in the atmosphere (that wasn't taken up in previous time steps by regrowing vegetation or by ocean exchange).

The atmospheric CO₂ anomaly resulting from the combined effect of the ocean and post-fire carbon sinks is shown in fig. S3D. Radiative forcing from CO₂ and CH₄ during years 0-80 (and reflecting this atmospheric CO₂ trajectory) was $1.6 \pm 0.8 \text{ W m}^{-2}$.

For this longer interval, our error estimate includes the components described above for year 1 as well as an additional 20% reflecting uncertainty introduced from estimating the post-fire atmospheric greenhouse gas trajectory.

1.5 Radiative forcing derived from observed changes in surface albedo

The instantaneous radiative forcing at the tropopause from a change in surface albedo due to fire is approximately equal to the difference in outgoing shortwave radiation between the control and burn sites, after this difference has been attenuated by clouds and other atmospheric constituents within the troposphere. Equivalently, it is the difference in net radiation at the tropopause caused by changes in surface albedo. We used the column radiation model (CRM; (25, 26)) to estimate net changes in tropopause radiation fluxes, starting with our measurements of surface albedo.

We constructed monthly mean estimates of incoming shortwave radiation (S_{in}) and outgoing shortwave radiation (S_{out}) from the Eppley precision spectral radiometers mounted on our towers (figs. S5 and S6). We constructed monthly mean values during 2002-2004, corresponding to a mean of years 3-5 after fire. Instrument heights and other details about our micrometeorological measurements are described by Liu et al. (12). The ratio of the monthly mean values of S_{out} and S_{in} were used to construct monthly mean values of surface albedo (fig. S7).

With CRM, we made four sets of model runs: with and without cloud cover and with control and burn surface albedo. For all simulations we used monthly mean profiles of atmospheric temperature, specific humidity, and ozone from the European Centre for Medium-Range Weather Forecasts 40 years Reanalysis product (27) and we assumed an aerosol optical depth of 0.14. For the cloud cover simulations, we imposed a single 100% cloud cover layer in the model at the 974 mb level, with a liquid water content of 100 g m⁻². For each set of model runs, we made a simulation for each hour of each month (a total of 288 simulations) to capture both diurnal and seasonal variations in solar geometry. We assumed the tropopause corresponded to the 198 mb level in the model.

Estimates of S_{in} at our sites from the clear sky and cloudy sky model simulations bracket our tower observations (fig. S5). We then solved for the clear sky and cloudy sky fractions each month that matched our monthly observations of S_{in} . These fractions were then used to combine the clear sky and cloudy sky model estimates of tropopause net radiation from the control and burn albedo simulations. Finally, we took the difference between tropopause net radiation between the control and burn albedo simulations (weighted by the appropriate clear sky and cloudy sky fractions) as our estimate of instantaneous radiative forcing at the tropopause (fig. S8). Based on a series of published climate simulations (2, 3) we assumed that stratospheric adjustment to changes in surface albedo was negligible and so the instantaneous forcing at the tropopause was equal to the IPCC definition of adjusted radiative forcing. In this analysis, we found that the difference in annual outgoing shortwave radiation at the tropopause was 60% of the difference in outgoing shortwave radiation at the surface.

Clouds, aerosols, and trace gases accounted for a 40% annual reduction of the outgoing surface signal using the CRM. The difference in S_{out} (control – burn) at the surface was -13.9 ± 3.0 W m⁻² (fig. S8). The difference at the tropopause, which is approximately equal to the radiative forcing from the surface albedo changes, was -8.4 W

m^{-2} . This value represents the mean from 2002-2004. Our error estimate for this forcing reflects both interannual variability in S_{out} caused by variations in snow cover ($\pm 1.8 \text{ W m}^{-2}$) and a subjective assessment of uncertainty introduced from the use of the CRM ($\pm 1.0 \text{ W m}^{-2}$) for a total of $\pm 2.8 \text{ W m}^{-2}$. For this period, 3-5 years after fire, summer albedo was higher in the recent burn than in the control from the establishment of grasses, small shrubs, and other changes in the surface. As a result, 24% of the annual radiative forcing was a result of fire-induced albedo changes during summer (May-September).

During the first year immediately following fire, the annual radiative forcing from surface albedo change was smaller than the 3-5 year mean. This was because charred surfaces and exposure of black carbon on the soil surface during the summer after the fire reduced albedo below that observed at nearby unburned conifer stands (28). After 3-5 years, the establishment of grasses, shrubs, and mosses and other changes to the surface increased summer albedo above pre-burn levels (Fig. 1). To estimate the radiative forcing during the first year, we assumed surface albedo within the Donnelly Flats perimeter in July, August, and September after the June 1999 fire was 0.07 (28). During winter and spring, and summer we used our observations (e.g., Fig. 1) to estimate surface albedo. We also assumed that the attenuation of outgoing shortwave radiation by clouds and atmospheric constituents was the same as for the 2002-2004 period: specifically that the difference in outgoing shortwave radiation at the tropopause was 60% of the difference at the surface. This yielded a year 1 albedo-driven radiative forcing of $-5.4 \pm 2.2 \text{ W m}^{-2}$, with the error estimate including $\pm 1.2 \text{ W m}^{-2}$ from uncertainty in the albedo measurements and $\pm 1.0 \text{ W m}^{-2}$ from a subjective assessment of the uncertainty associated with using the CRM.

1.6 Post-fire trajectory of surface albedo radiative forcing derived from MODIS

We extracted MODIS shortwave albedo (black sky and white sky) in interior Alaska to assess how long fire-induced changes in surface albedo persist during succession. The MODIS albedo product has a 16 day time step and a 1 km spatial resolution (29). Validation studies show that MODIS satellite-derived albedo agrees well with available field measurements, especially under snow-free conditions (30). Surface albedo was retrieved from the MODIS daily cloud-free atmospherically corrected directional surface reflectance using a semi-empirical bidirectional reflectance distribution model (BRDF) (31). The associated quality assurance fields are also stored in the operational product to provide information on the algorithm and product quality.

The black sky and white sky albedo products represent the fraction of radiation reflected by the surface under two extreme conditions. Black sky albedo represents the fraction of reflection when incoming light is in a direct beam whereas white sky albedo represents the fraction of reflection when the light source is isotropic diffuse. The albedo under realistic incoming solar radiation can be approximated as the combination of these two as a function of the fraction of direct and diffuse radiation (31, 32). Here we extracted the MODIS BRDF parameters to calculate the black sky albedo every 3 hours with the MODIS RossThickLiSparse BRDF model, since the MODIS black sky albedo was operationally produced only at local solar noon. The actual albedo was then derived as a sum of black sky albedo and white sky albedo weighted by the fraction of direct and diffuse surface incoming shortwave radiation. We used the monthly 3-hourly direct and

diffuse shortwave radiation data derived with the shortwave algorithm of the NASA World Climate Research Programme /Global Energy and Water-Cycle Experiment (WCRP/GEWEX) Surface Radiation Budget (SRB) Project (33). The radiation data were obtained from the Langley Atmospheric Sciences Data Center (http://eosweb.larc.nasa.gov/PRODOCS/srb/table_srb.html).

We identified burn perimeters using the Alaska fire history geographic information system (GIS) database from the Alaska Fire Service (AKFIREHIST; <http://agdc.usgs.gov/data/blm/fire/index.html>). In our analysis, we used fire perimeters from the beginning of the observed record (1950) through 2003 and MODIS data from 2000-2004. We excluded areas within 20 km of roads and towns to avoid post-fire trajectories that were substantially modified by human activity such as agriculture or development. We also imposed a 2 km buffer on the edge of burn perimeters to avoid possible geolocation errors. Another 1 pixel buffer on the outside of fire perimeters was excluded from our control areas (described below). Pixels identified as lakes, rivers, or water from a MODIS-derived vegetation cover map were also excluded (34). We also excluded pixels for a given time interval that did not pass MODIS quality assurance tests.

To derive the post-fire albedo trajectory, we calculated the mean albedo of all 1 km pixels that burned in a specific year for each 16-day MODIS interval. We did not include years for which there were fewer than 10 fire pixels or less than 2 fires. We constructed a pre-fire control albedo (shown by a dash dotted line in Fig. 2 in the main text) from the mean of all pixels within interior Alaska that did not burn during 1950-2003 and that were identified as evergreen conifer vegetation (34).

We assumed that the post-fire trajectory of albedo-driven radiative forcing followed MODIS albedo (Fig. 2A, dashed line, right axis). Albedo-driven radiative forcing increased from -5.0 W m^{-2} in year 1 to -8.5 W m^{-2} in year 10. During a deciduous phase (years 10-30), radiative forcing remained constant at -8.5 W m^{-2} reflecting sustained levels of elevated albedo during both spring and summer (Fig. 2). After year 30, radiative forcing decreased linearly, and was assumed to equal zero at year 55 and for all subsequent years. Averaged over years 0-80, albedo-driven radiative forcing was $-4.2 \pm 2.0 \text{ W m}^{-2}$. For this longer interval, our error estimate includes the components described above for years 3-5 (uncertainty from interannual variability in snow cover and use of the CRM) as well as an additional 20% reflecting uncertainty associated with estimating the post-fire trajectory of albedo from MODIS.

1.7 Ozone radiative forcing

The radiative forcing of ozone produced from the 2004 fire complex in Alaska and Yukon was estimated using the National Center for Atmospheric Research (NCAR) Community Atmosphere Model (CAM 3) by comparing model simulations that included fire emissions to a reference simulation where these emissions were turned off. The total fire emissions for the 2004 fire season were optimized weekly to match Measurements Of Pollution In The Troposphere (MOPITT) satellite observations of column CO over northern North America (35). This yielded total emissions of 30 Tg CO and a global annual mean O₃ atmospheric perturbation for the first year of 0.9 Tg O₃ – although most of the ozone was concentrated in the northern part of the northern hemisphere during summer. The burned area of the complex was approximately 4.45 x

10^{10} m^2 . When normalized to the carbon emissions estimates we obtained for the Donnelly Flats fire ($1560 \pm 610 \text{ g C m}^{-2}$), this led to an adjusted radiative forcing from ozone of 6 W per m^2 of burned area, with an error estimate of 4 W m^{-2} that included uncertainties in the emissions, the optimization (35), emission ratios (19), and the radiative transfer calculations. Our approach for obtaining the adjusted radiative forcing from the instantaneous forcing at the top of atmosphere (that was readily available from CAM 3) is provided in more detail in section 1.11 and table S1.

1.8 Instantaneous aerosol and snowpack radiative forcing

We simulated black carbon (BC) and organic carbon (OC) aerosol direct radiative forcing from the Donnelly Flats fire using CAM 3 (36). We used emissions described in section 1.1, applying BC and OC emission factors from M. Andreae ((19), pers. comm.), injected uniformly over the 8-day fire period. Aerosol optical properties were prescribed (37). Aerosols were injected into the lowest atmospheric layer, and hydrophobic BC and OC was transformed to hydrophilic components with an e-folding time of 1.2 days. We estimate global shortwave ($0.3\text{-}5.0 \mu\text{m}$) instantaneous top of atmosphere (TOA) radiative forcing from atmospheric BC and OC and surface forcing from BC in snow and ice with an ensemble of two 10 year simulations (fig. S9). In each simulation, fire emissions were injected into the model during June 11-18. Given that almost all of the instantaneous radiative forcing from both atmospheric aerosols and their deposition on snow and sea ice had dissipated after 6 months, this allowed for 10 independent model realizations within each run.

Snow radiative processes and aging were simulated with the SNow, ICe, and Aerosol Radiative model (SNICAR) (38), based on Warren and Wiscombe (39) and Toon et al. (40), and coupled to CAM 3. Factors which control snow and ice forcing include aerosol transport mechanisms, snow grain size, meltwater scavenging efficiency, BC optical properties, surface incident flux, and snow cover fraction. Very small quantities of BC can reduce snow reflectance (39, 41). For the changes in snow albedo caused by the deposition of BC, we assumed that instantaneous forcing at the tropopause was equal to 0.92 of the surface forcing based on a series of offline experiments with the Shortwave Narrowband (SWNB) atmospheric model (42) with varying albedo perturbation, cloud thickness, and aerosol absorption optical depth. We assumed that stratospheric readjustment was minimal, so that instantaneous tropopause forcing was approximately equal to the definition of radiative forcing given by the IPCC (2, 3).

About 89% of the direct radiative forcing from the atmospheric aerosols occurred immediately after the fire during the latter part of June. Another 11% occurred during July, with negligible contributions in subsequent months. The annual radiative forcing from atmospheric aerosols was $17 \pm 30 \text{ W m}^{-2}$. Our error estimate includes a large component caused by interannual variability in climate within CAM 3. Interannual variability in wind direction and strength at the point source, near-source snow and cloud conditions, and precipitation patterns influenced aerosol lifetimes and the strength of their forcing. At the surface, the perturbation to net shortwave radiation from both aerosol absorption and scattering was substantially larger and led to a net cooling of $-90 \pm 35 \text{ W m}^{-2}$.

The combined radiative forcing from BC deposition on snow and sea ice albedo was $8 \pm 5 \text{ W m}^{-2}$. Our error estimate includes interannual variability in model transport of BC to areas covered by snow and sea ice as well as uncertainty associated with modeling the radiative effects of BC on snow and ice albedo.

1.9 Stand age modeling

We constructed a grid with 1×10^5 cells, each with a unique age and each cell representing a single boreal forest stand. The probability of a cell burning (and having its age reset to zero) was set in the model to be a function of cell age. The probability of fire was suppressed in cells during the first 30 years and then increased to a constant final probability that remained constant for cells older than 55 years. The initial probability of fire was set equal to 1/5 of the final probability in our model simulations. This parameterization was based on an analysis of Alaskan burn perimeters (from the last 55 years (43)) that showed fires were more likely to occur in older rather than younger stands as compared to a probability distribution obtained from assuming fire did not depend on stand age. This parameterization generates a stand age distribution similar to that obtained from a Weibull function, which has been used in the past to model boreal forest stands (44). In terms of the underlying mechanism, suppression of fire in younger stands may occur from a delayed and slow build up of flammable fuels in the first few decades after fire and also from a higher water content of deciduous vegetation that often establishes immediately after fire (44).

In each model run, we stepped the model forward at 1 year increments out to 600 years. At each time step, the probability of fire in each cell was evaluated using the fire probability function described above (that was a function of the cell age) and a random number generator. At the end of each model run, we convolved the resulting stand age distribution with the post-fire trajectory of radiative forcing (for each agent) to compute a stand age-weighted radiative forcing mean.

For the greenhouse gas trajectories, we assumed a constant background CO_2 concentration (380 ppm) and we used ocean impulse functions from the pre-industrial period from Joos and Siegenthaler (24). These two adjustments were made (as compared to the approach taken in section 1.4) so that we could examine radiative forcing from a contemporary change in the fire regime in Fig. 3C. In a series of model runs, we varied the final probability of fire between 0.0055 and 0.03 at increments of 0.001. The resulting radiative forcing values are shown in Fig. 3C, assuming the stand age distribution starts at steady state with a mean fire return time of 80 years. We arbitrarily chose a mean of 80 years here for consistency with the stand age of our control - across the boreal biome fire return times vary widely (44). We could have added a different set of offsets so that the sum of different forcing agents was zero with a mean fire return time at steady state at 100 or 120 years. These adjustments would not change the slope of the lines in Fig. 3C or our conclusions. We also generated a series of stand age distributions assuming that the probability of fire did not depend on stand age (exponential distributions). These latter stand age distributions did not substantially change the slopes of the lines shown in Fig. 3C.

1.10 Other forcing agents

For the sake of brevity we did not consider several additional smaller forcing agents in the main text. Specifically, a small amount of heat is released directly from the oxidation of organic matter during combustion. Assuming fuels at Donnelly Flats had a heat of formation of 20.9 KJ/g and that organic matter was comprised of 50% carbon, the fire emissions pulse would have been accompanied by 65 MJ of heat released into the atmosphere. Averaged over year 1, this corresponds to 2 W m^{-2} , but not all of this would correspond to radiative forcing; some infrared radiation would be lost to space and would not contribute to atmospheric heating. Further, over 80 years, the net effect of this oxidation flux would be nearly zero because this is the time for biomass (and chemical energy) accumulation within the ecosystem to equal that lost during the initial fire event. We also did not consider aerosol indirect effects, including a reduction in cloud droplet size and extended cloud lifetimes. Although uncertain, the sum of all aerosol indirect effects are thought to contribute to a negative radiative forcing (1, 3, 45).

1.11 Approach for estimating adjusted and effective forcings

In the main text we report radiative forcing after the stratosphere has adjusted radiatively, following the IPCC TAR convention (1). This forcing, hereafter referred to as F_a , has been shown to be more closely linked with the equilibrium temperature response in climate models than other types of radiative forcing (2), but was not immediately available for a number of the agents that we examined here in the context of the Donnelly Flats fire. As a result, in some cases we needed to convert the instantaneous forcing at the top of atmosphere ($F_{i,toa}$) or at the tropopause ($F_{i,tropo}$) to F_a . For a number of agents, including post-fire albedo changes, BC deposition on snow and sea ice, and fire-emitted aerosols, the differences between $F_{i,toa}$, $F_{i,tropo}$, and F_a were relatively small. For ozone the differences were larger. We relied on our own radiative transfer modeling to convert between $F_{i,toa}$ and $F_{i,tropo}$, and then on published estimates from climate models (2, 3) to convert in a second step between $F_{i,tropo}$ and F_a . Hansen et al. (2) and Hansen et al. (3) provide background information on the relationship between these different types of radiative forcing, hereafter we refer to these two studies as H97 and H05.

We also report here in section 2 (SOM text) and in the footnote to Table 1 in the main text, the effective forcing from the different agents, taking into account that the global temperature response per unit of forcing varies depending on the agent (3). Note that the efficacy values we report in Table S1 are relative to F_a and are derived from H05.

Myhre et al. (23) provide equations for directly computing F_a from atmospheric concentrations of CO_2 and CH_4 and so we did not need to convert between instantaneous and adjusted forcings. The efficacy of forcing agents is defined relative to the forcing from CO_2 , so by definition CO_2 has an efficacy of 1.0 (3). The efficacy for methane is approximately 1.45 because methane indirectly contributes to stratospheric water vapor and tropospheric ozone (3).

For ozone, we estimated $F_{i,toa}$ from simulations with the NCAR Community Atmosphere Model (CAM 3) as described in section 1.7 above. We then used the vertical profile of the ozone anomaly from CAM 3 with the CRM model (described in section 1.5) to estimate $F_{i,tropo}$. In a second step, we assumed that the ratio of $F_{i,tropo}$ to F_a from ozone emitted from the Donnelly Flats fire was the same as that derived from

tropospheric ozone simulations with the GISS model (3). The efficacy for forcing associated with increases in tropospheric ozone is approximately 0.82 (3).

To estimate F_a from BC deposition on remote snow and sea ice, we first obtained $F_{i,tropo}$ based on the approach is described in section 1.8. In a second step, we assumed that $F_{i,tropo}$ was equal to F_a for snow and sea ice forcing from Donnelly Flats fire based on climate model simulations of changes in surface albedo (as shown in Table 11 of H97). The efficacy for black carbon deposition is thought to be relatively large (1.7) because of snow and ice feedbacks (3).

To estimate F_a from aerosols emitted by the Donnelly Flats fire, we first obtained $F_{i,toa}$ from the CAM 3 (the approach is described in section 1.8). Based on simulations from the SWNB model, we estimated that $F_{i,tropo}$ was slightly larger than $F_{i,toa}$ ($F_{i,tropo} = F_{i,toa} * 1.01$). In a second step, we assumed that $F_{i,tropo}$ was approximately equal to F_a for aerosol forcing from the Donnelly Flats fire based on global climate model simulations with tropospheric aerosols (Table 10 from H97 and Table 2 from H05). For aerosols, we used an efficacy of -0.2 based on Table 5 of H05. This value was negative because forcing from OC aerosols has a substantially higher efficacy (0.91) than forcing from BC aerosols (0.58). More specifically, because the net forcing from biomass burning aerosols reflects a balance between a large positive component associated with absorptive BC and a large negative component associated with reflective OC, a smaller efficacy for the positive term can flip the sign of the net effective forcing.

To estimate F_a from the changes in surface albedo within the Donnelly Flats burn perimeter, we first obtained $F_{i,tropo}$ from CRM, driving the model with observations of surface albedo and incoming shortwave radiation at our field sites (the approach is described in section 1.5). As with the snow and sea ice forcing approach described above, in a second step we assumed that the ratio $F_{i,tropo}$ was the same as F_a based on northern surface albedo simulations obtained from a global climate model (Table 11 from H97).

2. Supporting text

Feedbacks We used the concept of radiative forcing to compare the different ways by which fire influences climate. As noted in the main text an important next step is to quantify feedbacks. One important feedback that may contribute to cooling with increased fire activity is the replacement of conifer stands with broadleaf deciduous stands. High mid-summer evapotranspiration fluxes associated with broadleaf deciduous trees (12, 28, 46) may increase cloud cover and planetary albedo, and thus contribute to additional cooling.

In contrast, over centennial to millennial time scales, increased deposition of black carbon on sea ice and the Greenland ice sheet may accelerate surface melting and mass loss. Reductions in aerial extent of the Greenland ice sheet would substantially decrease northern albedo and thus would represent a strong positive feedback to warming (apart from impacts on sea level and ocean circulation).

Effective forcings Following the approach by H05, we also estimated effective forcings (F_e). These forcings were obtained by multiplying the adjusted forcings in Table 1 of the main text (F_a) by the efficacy values reported in Table S1. In terms of F_e , the net effect of the Donnelly Flats fire was $-2.4 \pm 2.3 \text{ W m}^{-2}$ over the 80-year fire cycle (Table S2), reflecting a slightly larger cooling impact of fire than what we obtained from the total adjusted forcing ($-2.3 \pm 2.2 \text{ W m}^{-2}$ as reported in Table 1 of the main text).

3. Supporting figures



Fig S1. Photo of the Donnelly Flats fire that occurred during 11-18 June 1999. This photo was taken on 13 June 1999 from Fort Greely looking south towards the fire front and the Alaska Range. Photo credit: Kerensa Hardy, Ft. Greely Public Affairs, U.S. Army. Reproduced by permission of the Delta News Web.



Fig S2. Photo of the Donnelly Flats fire on Fort Greely. Photo credit: Tom Lucas. Reproduced by permission of the Delta News Web.

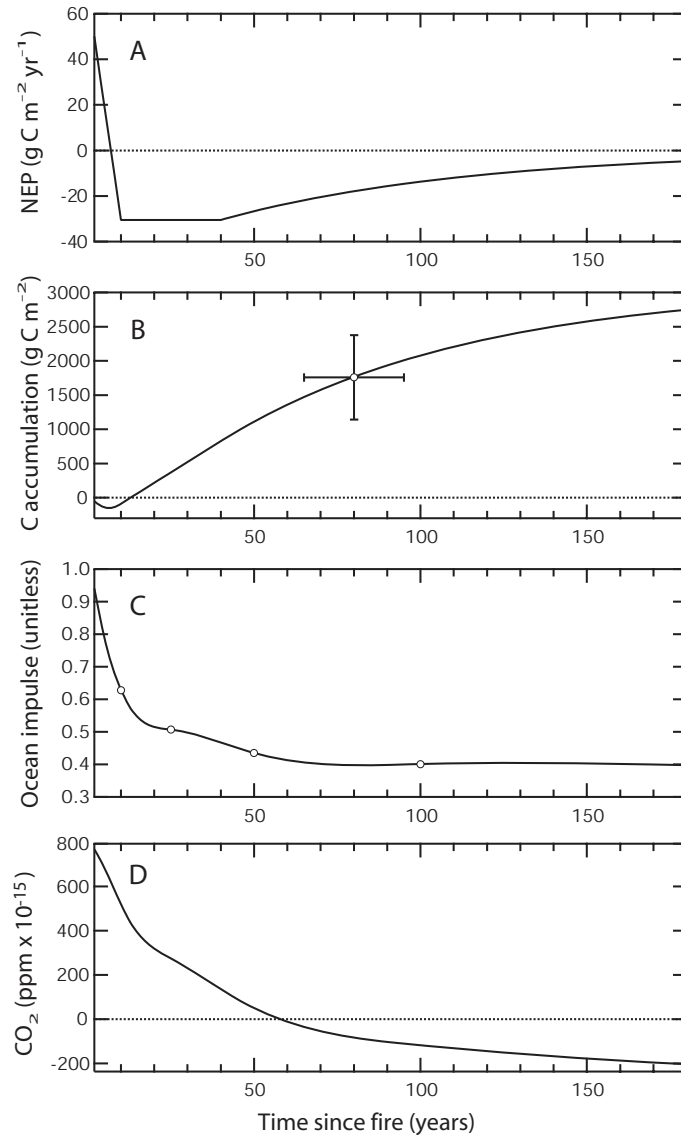


Fig. S3. A) Trajectory of net ecosystem production (NEP) constructed with the constraint that carbon accumulation over the first 80 years was equal to carbon loss during the first year of the Donnelly Flats fire and that uptake rates were highest during a deciduous phase from 10 to 40 years. B) Trajectory of total carbon accumulation (the integral of A). The point represents the measured total carbon loss during the Donnelly Flats fire and was obtained by a comparison of carbon inventories within the burn perimeter to carbon inventories from the approximately 80-year adjacent control stand. C) The fraction of atmospheric CO_2 pulse (injected at time 0 and with strength of 1 unit) that remains airborne as a function of time, as a result of ocean-atmosphere gas exchange. This impulse function was constructed assuming the injection occurred during contemporary times (during the 1990s) and that CO_2 concentrations continue to increase until they stabilize at 650 ppm at the end of the century (24). D) The global CO_2 anomaly from the Donnelly Flats fire (per m^2 of emissions). This anomaly reflects uptake of the fire CO_2 pulse by both the oceans and by regrowing vegetation within the fire scar.

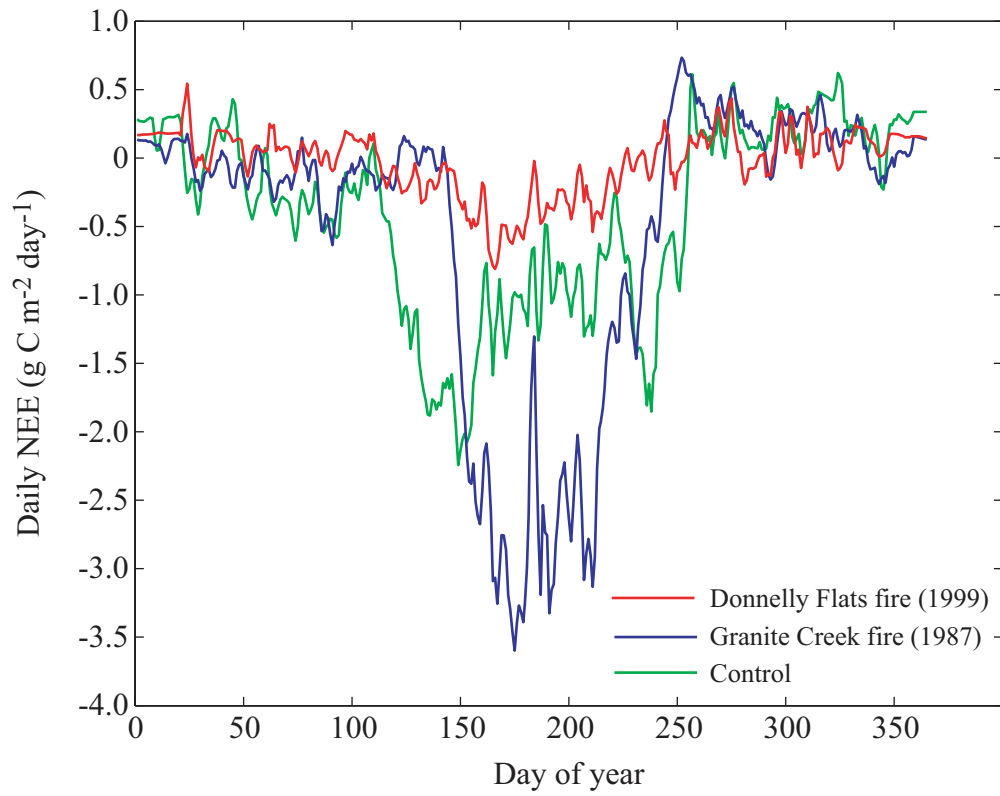


Fig. S4. Daily net ecosystem exchange measured by eddy covariance at the Donnelly Flats fire (1999), the Granite Creek fire (1987), and the control stand averaged over 2002-2004.

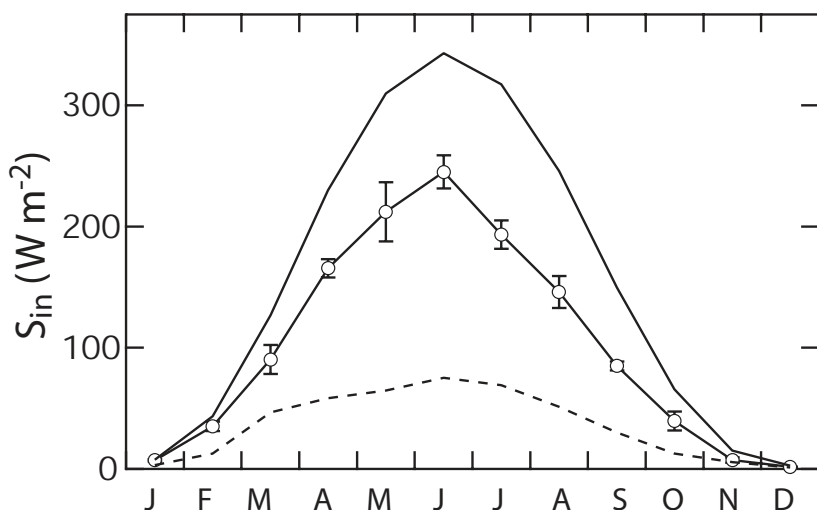


Fig. S5. Observations of incoming shortwave radiation (S_{in}) from our field sites near Delta Junction, Alaska (circles with standard deviation error bars) fall in between column radiation model (CRM) estimates for clear sky (solid line) and cloudy conditions (dashed line). The measurements of S_{in} represent the monthly mean of 3 years (2002-2004) from two radiometers (one at each of the burn and control sites). Standard deviation error bars primarily reflect interannual variability in cloudiness for a given month.

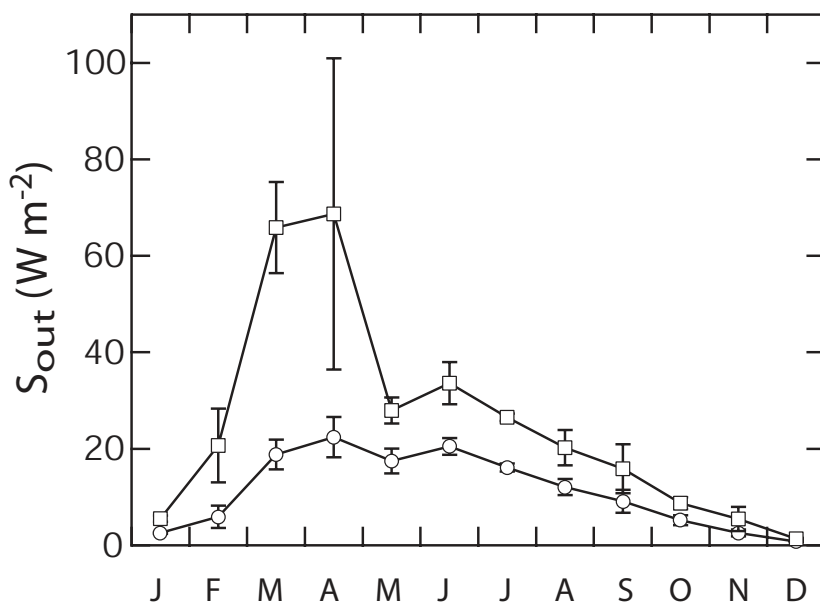


Fig. S6. Observations of outgoing shortwave radiation (S_{out}) from the control (circles) and burn (squares), measured using radiometers above the canopy and averaged over 2002-2004. The difference in S_{out} at the tropopause (after attenuation by clouds and other atmospheric constituents in the troposphere) is approximately equal to the radiative forcing from the fire-induced change in surface albedo. Interannual variability in S_{out} (shown with the standard deviation error bars) was greatest during April, primarily as a result of year-to-year differences in the timing of snowmelt.

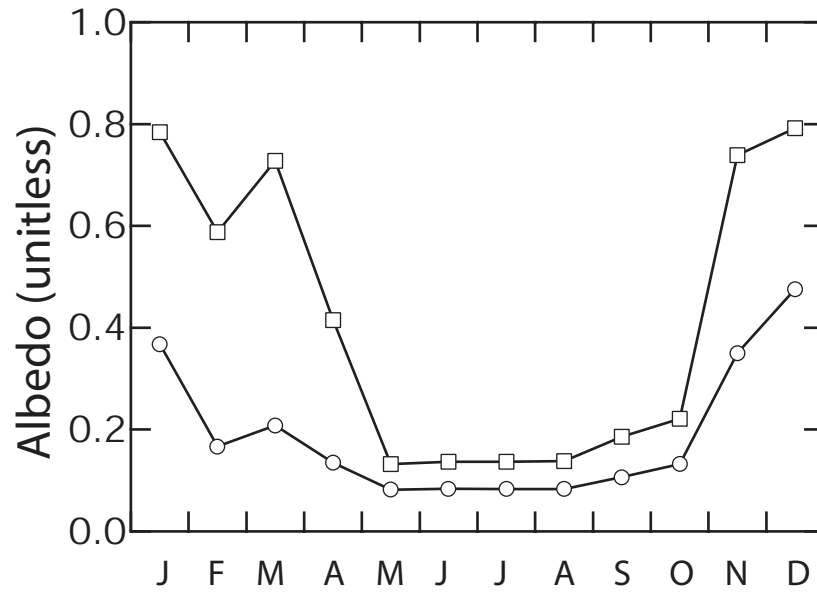


Fig. S7. Monthly mean surface albedo from the control stand (circles) and from within the Donnelly Flats burn perimeter (squares) during 2002-2004.

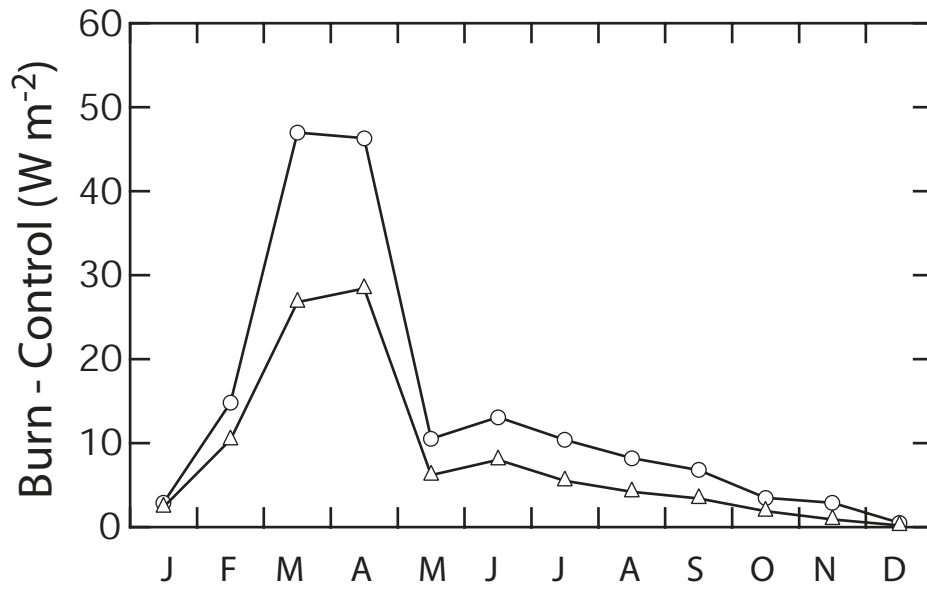


Fig. S8. Difference in outgoing shortwave radiation between the burn and control at the surface (circles) and at the tropopause (triangles). The tropopause shortwave radiation difference was estimated using the Column Radiation Model described in the Supporting Online Methods section 1.5.

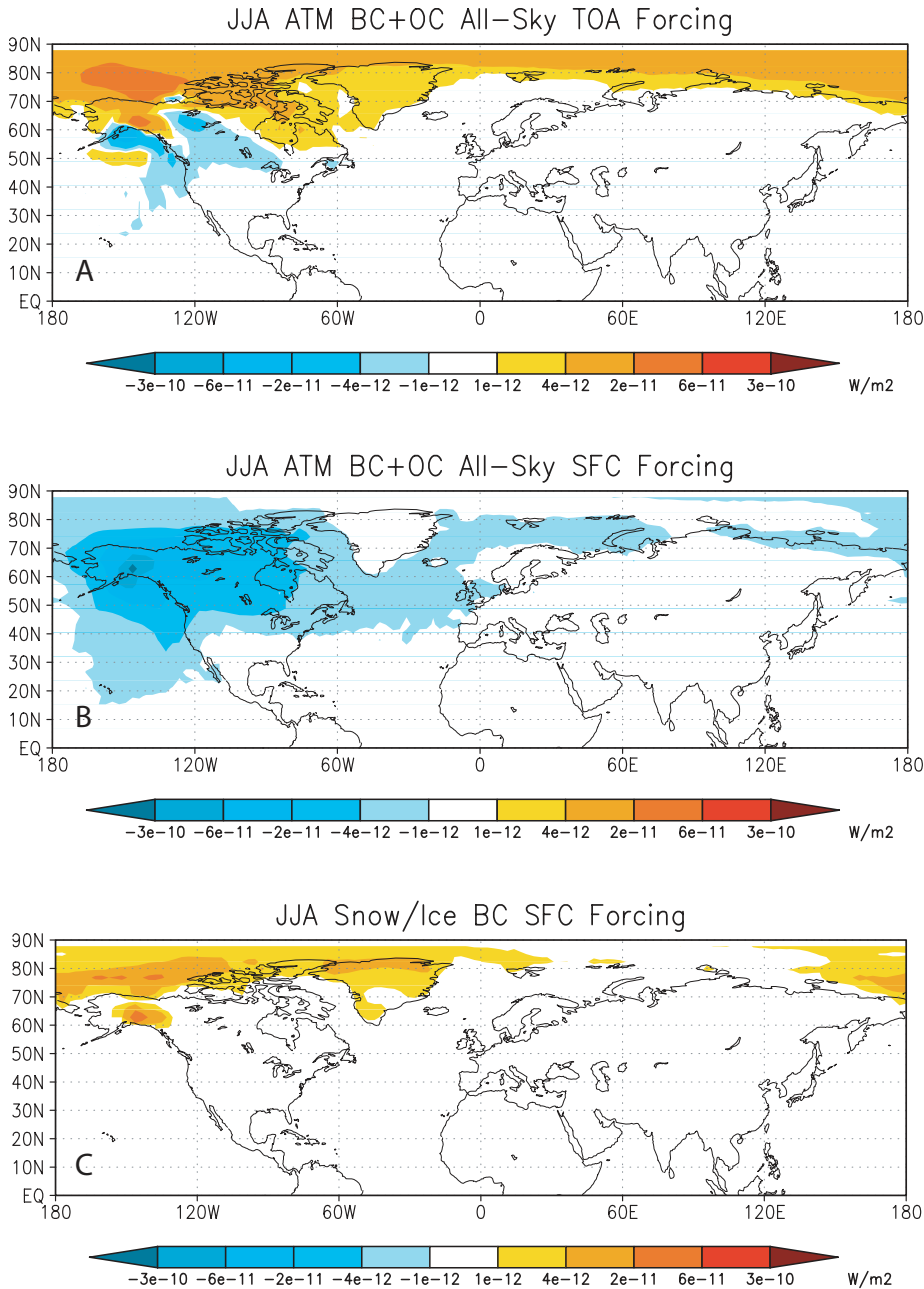


Fig. S9. A) Top of atmosphere instantaneous radiative forcing from aerosols emitted from the Donnelly Flats fire for all-sky conditions (including both clear sky and cloudy conditions) was concentrated primarily in boreal and arctic regions. B) At the surface, the perturbation to net shortwave radiation from both aerosol absorption and scattering was substantial and led to a net cooling of -90 ± 35 W per m^2 of burned area. C) Surface forcing from black carbon deposition primarily occurred on sea ice, the Greenland ice sheet, and snow in the Alaska Range. All of these estimates were derived from the NCAR CAM 3. Note that the color scale is logarithmic.

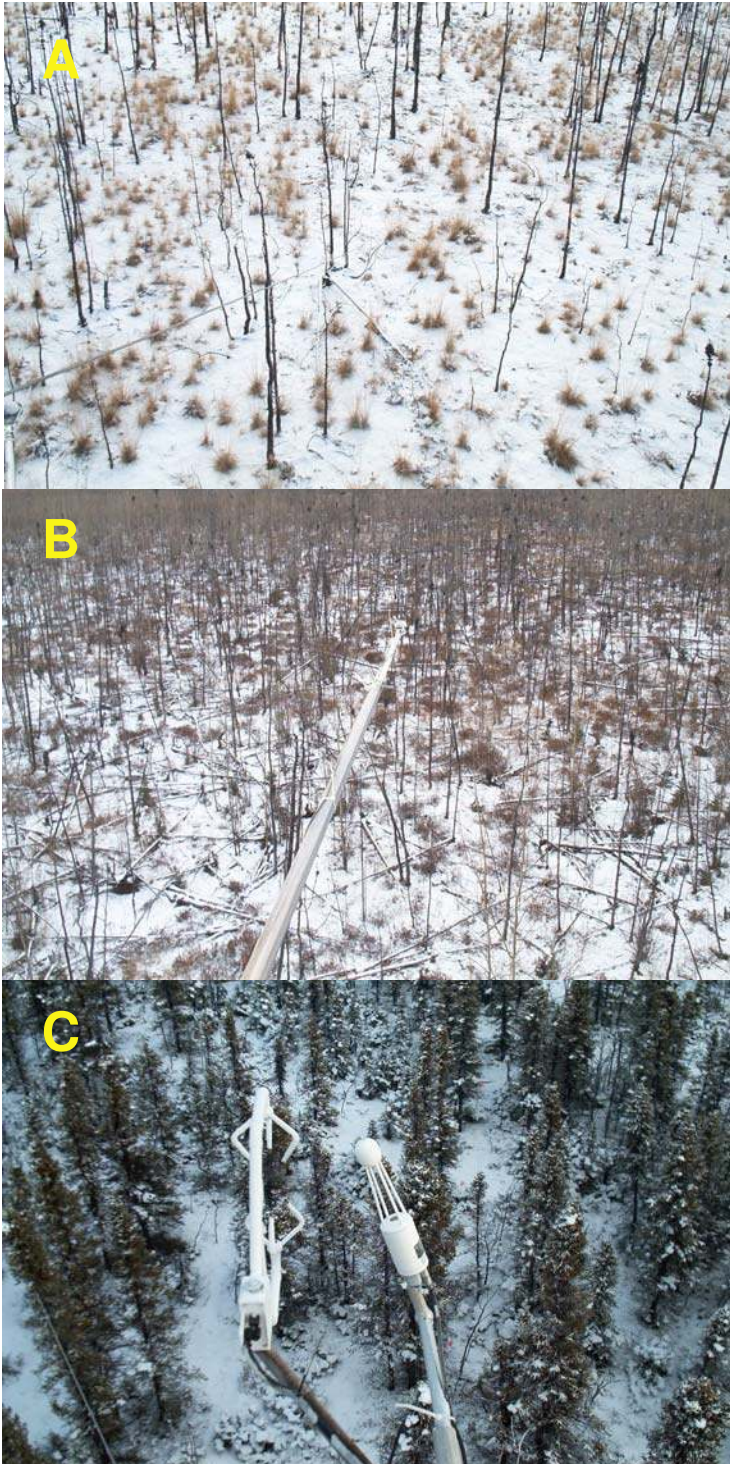


Fig. S10. Photographs of the Donnelly Flats stand that burned in 1999 (A), the Granite Creek stand that burned in 1987 (B), and the control stand that burned in approximately 1920. These photographs were taken from the eddy covariance towers at these sites on 30 November 2002.

4. Supporting tables

Table S1. The relationship between different forcing estimates and their efficacy

Agent	$F_{i,tropo}^a / F_{i,toa}$	$F_a / F_{i,tropo}$	Efficacy ^b
Greenhouse gases			
CO ₂	N/A	N/A	1.00
CH ₄	N/A	N/A	1.45
Ozone	1.30	0.83	0.82
Black carbon deposition on snow	N/A	1.00	1.7
Black carbon deposition on sea ice	N/A	1.00	1.7
Aerosols (net)	1.01	1.00	-0.20
black carbon	1.01	1.04	0.58
organic carbon	1.01	0.98	0.91
Changes in post-fire surface albedo	N/A	1.00	1.02

- a. $F_{i,tropo}$ is the instantaneous radiative forcing at the tropopause, $F_{i,toa}$ is the instantaneous radiative forcing at the top of atmosphere, and F_a is the adjusted forcing (the IPCC TAR convention).
- b. We obtained these efficacy estimates from H05.

Table S2. Effective radiative forcing (F_e) associated with the Donnelly Flats fire

Forcing agent:	Radiative forcing ^a , W (m ² burned) ⁻¹	
	Year 1	Years 0-80 (mean)
Long-lived greenhouse gases (CO ₂ and CH ₄)	9 ± 4	1.7 ± 0.9
Ozone	5 ± 4	0.1 ± 0.0
Black carbon deposition on snow	5 ± 5	0.1 ± 0.1
Black carbon deposition on sea ice	9 ± 7	0.1 ± 0.1
Aerosols (direct radiative forcing) ^b	-3 ± 40	0.0 ± 0.5
Impact at the surface: -90 W ± 35 m ⁻²		
Changes in post-fire surface albedo	-5 ± 2	-4.3 ± 2.1
Total	18 ± 41	-2.4 ± 2.3

- a. Radiative forcing here refers to effective forcing (F_e) following the approach described by Hansen et al. (2005) and as described in section 1.11. Efficacy values from Table S1 were applied to the adjusted forcing estimates provided in Table 1 of the main text.
- b. The aerosol forcing changed sign from 17 W m⁻² to -3 W m⁻² and the uncertainties increased as a result of applying the efficacy values from Table S1.

5. Supporting references and notes

1. V. Ramaswamy *et al.*, in *Climate Change 2001: The Scientific Basis. Contributions of Working Group I to the Third Assessment Report of the Intergovernmental Panel on Climate Change* J. T. Houghton *et al.*, Eds. (Cambridge University Press, Cambridge, United Kingdom and New York, NY, USA, 2001) pp. 350-416.
2. J. Hansen, M. Sato, R. Ruedy, *Journal of Geophysical Research-Atmospheres* **102**, 6831 (1997).
3. J. Hansen *et al.*, *Journal of Geophysical Research-Atmospheres* **110**, 10.1029/2005JD005776 (2005).
4. T. R. Crow, *Ecology* **59**, 265 (1978).
5. J. C. Neff, J. W. Harden, G. Gleixner, *Canadian Journal of Forest Research- Revue Canadienne De Recherche Forestiere* **35**, 2178 (2005).
6. D. U. Hooper, Z. I. Cardon, C. F. S. III, M. Durant, *Oecologia* **132**, 1 (2002).
7. E. K. Webb, G. I. Pearman, R. Leuning, *Quarterly Journal of the Royal Meteorological Society* **106**, 85 (1980).
8. D. D. Baldocchi, B. B. Hicks, T. P. Meyers, *Ecology* **69**, 1331 (1988).
9. T. W. Horst, *Boundary-Layer Meteorology* **82**, 219 (1997).
10. W. Eugster, W. Senn, *Boundary-Layer Meteorology* **74**, 321 (1995).
11. S. D. Chambers, J. M. Hacker, A. G. Williams, "The RAMF Users' Manual (Version 8.1)." *Tech. Report No. Technical Report No. 14.* (The Flinders University of South Australia, 1996).
12. H. P. Liu, J. T. Randerson, J. Lindfors, F. S. Chapin, *Journal of Geophysical Research-Atmospheres* **110**, 10.1029/2004JD005158 (2005).
13. L. R. Welp, J. T. Randerson, H. P. Liu, *Journal of Geophysical Research-Biogeosciences* **111**, 10.1029/2005JG000126 (2006).
14. M. L. Goulden *et al.*, *Science* **279**, 214 (1998).
15. S. E. Trumbore, J. W. Harden, *Journal of Geophysical Research-Atmospheres* **102**, 28817 (1997).
16. B. Bond-Lamberty, C. K. Wang, S. T. Gower, *Global Change Biology* **10**, 473 (2004).
17. K. P. O'Neill, E. S. Kasischke, D. D. Richter, *Journal of Geophysical Research-Atmospheres* **108**, 10.1029/2001JD000443 (2003).
18. F. S. I. Chapin *et al.*, *Ecosystems* **In Press**. (2006).
19. M. O. Andreae, P. Merlet, *Global Biogeochemical Cycles* **15**, 955 (2001).
20. T. M. Butler, P. J. Rayner, I. Simmonds, M. G. Lawrence, *Journal of Geophysical Research-Atmospheres* **110**, 10.1029/2005JD006071. (2005).
21. J. S. Daniel, S. Solomon, *Journal of Geophysical Research-Atmospheres* **103**, 13249 (1998).
22. M. J. Prather, *Geophysical Research Letters* **23**, 2597 (1996).
23. G. Myhre, E. J. Highwood, K. P. Shine, F. Stordal, *Geophysical Research Letters* **25**, 2715 (1998).

24. I. G. Enting, T. M. L. Wigley, M. Heimann, "Future Emissions and Concentrations of Carbon Dioxide: Key Ocean/Atmosphere/Land Analyses" (Technical paper no. 31, CSIRO Division of Atmospheric Research, 2001).
25. B. P. Briegleb, *Journal of Geophysical Research-Atmospheres* **97**, 7603 (1992).
26. J. T. Kiehl *et al.*, "Description of NCAR Community Climate Model (CCM3)" *Tech. Report No. TN-420* (National Center for Atmospheric Research, 1996).
27. S. M. Uppala *et al.*, *Quarterly Journal of the Royal Meteorological Society* **131**, 2961 (2005).
28. S. D. Chambers, F. S. Chapin, *Journal of Geophysical Research-Atmospheres* **108**, 10.1029/2001JD000530 (2002).
29. C. B. Schaaf *et al.*, *Remote Sensing of Environment* **83**, 135 (2002).
30. Y. F. Jin *et al.*, *Journal of Geophysical Research-Atmospheres* **108**, 10.1029/2002JD002803 (2003).
31. W. Lucht, C. B. Schaaf, A. H. Strahler, *Ieee Transactions on Geoscience and Remote Sensing* **38**, 977 (2000).
32. P. Lewis, M. Barnsley, paper presented at the International Symposium on Physical Measurements and Signatures in Remote Sensing, Int. Soc. for Photogramm. and Remote Sens., Val d'Isere, France. 1994.
33. R. T. Pinker, I. Laszlo, *Journal of Climate* **5**, 56 (1992).
34. M. A. Friedl *et al.*, *Remote Sensing of Environment* **83**, 287 (2002).
35. G. Pfister *et al.*, *Geophysical Research Letters* **32**, 10.1029/2005GL022995 (2005).
36. P. J. Rasch, W. D. Collins, B. E. Eaton, *Journal of Geophysical Research-Atmospheres* **106**, 7337 (2001).
37. M. Hess, P. Koepke, I. Schult, *Bulletin of the American Meteorological Society* **79**, 831 (1998).
38. M. G. Flanner, C. S. Zender, *Journal of Geophysical Research* **111**, D12208 (2006).
39. S. G. Warren, W. J. Wiscombe, *Journal of the Atmospheric Sciences* **37**, 2734 (1980).
40. O. B. Toon, C. P. McKay, T. P. Ackerman, K. Santhanam, *Journal of Geophysical Research-Atmospheres* **94**, 16287 (1989).
41. A. D. Clarke, K. J. Noone, *Atmospheric Environment* **19**, 2045 (1985).
42. C. S. Zender *et al.*, *Journal of Geophysical Research-Atmospheres* **102**, 29901 (1997).
43. The Alaska Fire Service maintains a database of annual fire statistics and geographic information system (GIS) burn perimeters (<http://agdc.usgs.gov/data/blm/fire/>).
44. E. A. Johnson, *Fire and Vegetation Dynamics: Studies from the North American Boreal Forest*. H. J. B. Birks, Ed., Cambridge Studies in Ecology (Cambridge University Press, 1992), pp. 127.
45. V. Ramanathan, P. J. Crutzen, J. T. Kiehl, D. Rosenfeld, *Science* **294**, 2119 (2001).
46. D. Baldocchi, F. M. Kelliher, T. A. Black, P. Jarvis, *Global Change Biology* **6**, 69 (2000).

[CO₂]- and density-dependent competition between grassland species

MARK VAN KLEUNEN*†, M. ANDRE STEPHAN* and BERNHARD SCHMID*

*Institute of Environmental Sciences, University of Zurich, Winterthurerstrasse 190, CH-8057 Zurich, Switzerland, †School of Biological and Conservation Sciences, University of KwaZulu-Natal, PO Bag X01 Scottsville, Pietermaritzburg 3209, South Africa

Abstract

The predicted ongoing increase of atmospheric carbon dioxide levels is considered to be one of the main threats to biodiversity due to potential changes in biotic interactions. We tested whether effects of intra- and interspecific planting density of the calcareous grassland perennials *Bromus erectus* and *Carex flacca* change in response to elevated [CO₂] (600 ppm) by using factorial combinations of seven densities (0, 1, 2, 4, 8, 16, 24 tillers per 8 × 8 cm² cell) of both species in plots with and without CO₂ enrichment. Although aboveground biomass of *C. flacca* was increased by 54% under elevated [CO₂], the combined aboveground biomass of the whole stand was not significantly increased. *C. flacca* tended to produce more tillers under elevated [CO₂] while *B. erectus* produced less tillers. The positive effect of [CO₂] on the number of tillers of *C. flacca* was strongest at high intraspecific densities. On the other hand, the negative effect of [CO₂] on the number of tillers of *B. erectus* was not present at intermediate intraspecific planting densities. Seed production of *C. flacca* was more than doubled under elevated [CO₂], while seed production of *B. erectus* was not affected. Moreover, the mass per seed of *C. flacca* was increased by elevated [CO₂] at intermediate interspecific planting densities while the mass per seed of *B. erectus* was decreased by elevated [CO₂] at high interspecific planting densities. Our results show that the responses of *C. flacca* and *B. erectus* to elevated [CO₂] depend in a complex way on initial planting densities of both species. In other words, competition between these two model species is both [CO₂]- and density dependent. On average, however, the effects of [CO₂] on the individual species indicate that the composition of calcareous grasslands is likely to change under elevated [CO₂] in favor of *C. flacca*.

Keywords: biotic interactions, calcareous grassland, carbon dioxide, clonal growth, competition, FACE, fan design, global change, plant density, response surface

Received 10 February 2006; revised version received 10 July 2006 and accepted 30 May 2006

Introduction

During the second half of the 20th century, the atmospheric carbon dioxide level ([CO₂]) has steadily risen (Keeling, 1993), and is predicted to further rise from its ambient concentration of around 375 ppm to a value between 540 and 970 ppm by the end of the 21st century (IPCC, 2001). Because CO₂ is one of the main resources for plant growth, the predicted increase in atmospheric [CO₂] is likely to affect interactions between species.

Therefore, elevated [CO₂] is considered to be one of the main components of global change that may threaten biodiversity (Peters & Lovejoy, 1992).

Most plants produce more biomass when grown at elevated [CO₂] but there is considerable variation in biomass gain among species (Hunt *et al.*, 1991; Poorter *et al.*, 1996; Poorter & Navas, 2003) and among genotypes (Leadley & Stöcklin, 1996; Schmid *et al.*, 1996; Steinger *et al.*, 1997). Therefore, it is likely that an increase of atmospheric [CO₂] will result in changes in both inter- and intraspecific competition. This might indirectly result in negative rather than positive effects of elevated [CO₂] on some species and, thereby change the composition of plant communities (Körner & Bazzaz, 1996). Indeed, several studies have shown that

Correspondence: Mark Van Kleunen, School of Biological and Conservation Sciences, University of KwaZulu-Natal, PO Bag X01 Scottsville, Pietermaritzburg 3209, South Africa, tel. +27 332 605 657, fax +27 332 605 105, e-mail: vankleunen@ukzn.ac.za

when plants are grown in competition, their carbon gain under elevated [CO₂] is less than when they are grown in isolation (Navas, 1998; Poorter & Navas, 2003). This implies that it is not possible to use the responses to elevated [CO₂] of isolated plants for predicting which species will increase under elevated [CO₂] and which ones will decline (Diaz, 1995; Körner, 1995; Warwick *et al.*, 1998; Navas *et al.*, 1999).

In the last few decades, several studies have confirmed that both intra- (e.g. Bazzaz *et al.*, 1992; Firbank *et al.*, 1995; Wayne *et al.*, 1999) and interspecific (e.g. Bazzaz & Garbutt, 1988; Dukes, 2002; Hely & Roxburgh, 2005) interactions are likely to change under elevated [CO₂]. Most of these studies tested for effects of elevated [CO₂] on intra- and interspecific competition separately, used only few levels of total density and often only equal frequencies of species in mixtures (Navas, 1998, but see Ramseier *et al.*, 2005 for an exception). Because responses to intra- and interspecific competition may be nonlinear and interact, results of such studies are difficult to extrapolate to the different densities and frequencies of species found in nature. Therefore, experiments are required that test plant responses under a wide range of densities and frequencies of the species (Law & Watkinson, 1987; Inouye, 2001).

Most studies quantified the effect of elevated [CO₂] and competition on plants in terms of biomass production (e.g. Hunt *et al.*, 1991; Poorter & Navas, 2003). Changes in biomass production are important short-term responses to changing [CO₂] but the ultimate ecological and evolutionary consequences of increasing [CO₂] will be mediated by differences in reproduction (Strain & Bazzaz, 1983). Although effects of intra- and interspecific competition on reproductive allocation have been frequently studied (van Kleunen *et al.*, 2001, 2002 and references therein), only few studies tested for effects of elevated [CO₂] on reproductive allocation (Garbutt & Bazzaz, 1984; Hikosaka *et al.*, 2005).

We tested for changes in intra- and interspecific competition in response to [CO₂] in the two calcareous grassland perennials *Bromus erectus* and *Carex flacca*. Calcareous grassland is one of the most species-rich vegetation types in Europe (Zoller, 1954; Willems, 1992; Fischer & Stöcklin, 1997), and in Central Europe it is mainly dominated by the clonal grass *B. erectus* whereas the clonal sedge *C. flacca* is subdominant in these habitats (Stöcklin *et al.*, 1998). Previous studies have shown that in these communities, *C. flacca* becomes more dominant under elevated [CO₂] (Leadley & Körner, 1996; Diaz *et al.*, 1998; Stöcklin *et al.*, 1998) while the dominance of *B. erectus* is not affected (Leadley & Körner, 1996; Leadley & Stöcklin, 1996) or decreases (Stöcklin *et al.*, 1998). This suggests, that under elevated [CO₂], competitive interactions between both species may change in favor of *C. flacca*.

To address whether whole community productivity and competition between *B. erectus* and *C. flacca* change under elevated [CO₂] and with planting density, we asked the following specific questions: (1) Does the combined aboveground biomass of *B. erectus* and *C. flacca* increase under elevated [CO₂]? (2) Do aboveground biomass and vegetative and sexual reproduction increase more strongly in *C. flacca* than in *B. erectus* under elevated [CO₂]? (3) How do intra- and interspecific planting densities affect the response of each species to elevated [CO₂]?

Methods

Study species

B. erectus (Poaceae) is a perennial grass which typically occurs in semi-arid grasslands on nutrient-poor calcareous soils (Ellenberg, 1986) where it is often the dominant species. New tillers are produced from meristems in the axils of leaves. As a consequence, genets form dense tussocks. Nonreproductive tillers are usually up to 40 cm tall, while reproductive tillers may reach a height of 1 m. Each reproductive tiller carries usually five to 20 spikelets, and each spikelet produces five to 10 flowers.

C. flacca is a perennial sedge which occurs in a wide range of open grassland habitats but often on soils containing free carbonate. The species often cooccurs with *B. erectus* in calcareous grasslands. New tillers are produced along rhizomes at relatively long distances from each other. As a consequence, genets have a spreading growth form of which the tillers are intermingled with the other plants. Tillers can grow up to 60 cm. Each reproductive tiller carries usually two to three female spikelets, and each spikelet can produce about 100 flowers.

Plant material and precultivation

In April 1997, we collected for both species a total of 20 000 tillers from three research fields in the Jura mountains close to Basel, Switzerland. We transferred clumps of tillers to a greenhouse, separated them into single or pairs of tillers, and planted them in 8 × 8 × 6 cm³ pots filled with a mixture of 60% soil from the Jura Mountains, 30% washed sand and 10% chalk marl according to a factorial design with seven density levels of both species (0, 1, 2, 4, 8, 16 and 24 tillers per cell). One day before the plants were transferred to the experimental field, we standardized their aboveground size by cutting all tillers back to 3 cm above soil level. To minimize transplant stress, we did not remove rhizosphere soil and did not cut the roots. Thus,

belowground size was not standardized any further than via using similar volumes of attached soil.

Experimental setup

The experiment took place in a grassland with three rings of free air carbon dioxide enrichment (FACE rings, Hendrey *et al.*, 1993) in Eschikon, Switzerland (47°27'N, 8°41'E, 550 m a.s.l.) each paired with a control ring of the same size without CO₂-enriched air (i.e. six rings in total). Each FACE ring consisted of an open circular area of 18 m diameter in which CO₂-enriched air was released during the day period of the growing season to increase the [CO₂] in the ring to 600 ppm. FACE rings were separated by at least 100 m.

In the middle of each of the six rings, we created an experimental plot of calcareous soil with four 0.8 × 0.8 m² quadrants (i.e. 24 quadrants in total). To create soil conditions similar to the ones in calcareous grasslands, we removed the 25 cm top layer of natural soil in each quadrant, and replaced it with a 1 cm thick layer of chalk mark on which we put an 18 cm thick layer of a mixture of commercial potting compost, sand, Styromull and chalk powder. The upper 6 cm layer consisted of the calcareous soil from the pots in which we had precultivated the plants. We separated the quadrants from the surrounding natural soil to a depth of 25 cm with PVC plates.

In each of the quadrants, which consisted of one hundred 8 × 8 cm² cells, we created between May 6 and August 22 1997 a density gradient of *B. erectus* and an orthogonal density gradient of *C. flacca* by arranging the 8 × 8 × 6 cm³ pots containing different ratios and tiller densities of both species in such a way that the number of tillers per cell increased in one direction from 0–0–0–1–2–4–8–16–24–24 for *B. erectus* and the same in the perpendicular direction for *C. flacca* (Fig. 1). Pots were removed before planting. This way we had each species as a monoculture at each of the densities as well as mixtures of both species at each of the planting density combinations. Because the cells on the outside served as buffer for the whole quadrant, and the third row and column served as buffers to separate the monocultures of each species from the mixture (Fig. 1), we had one experimental cell for each planting density and species combination per quadrant. To reduce the large amount of labor involved in the setup of the experiment, we did not use buffer rows between the different mixtures. To avoid bias due to geographical orientation of the density gradient, we randomized the four possible directions of the gradient between the four quadrants in each plot. For each of the six plots, we, thus, had four replicates of each combination of planting densities of the two species.

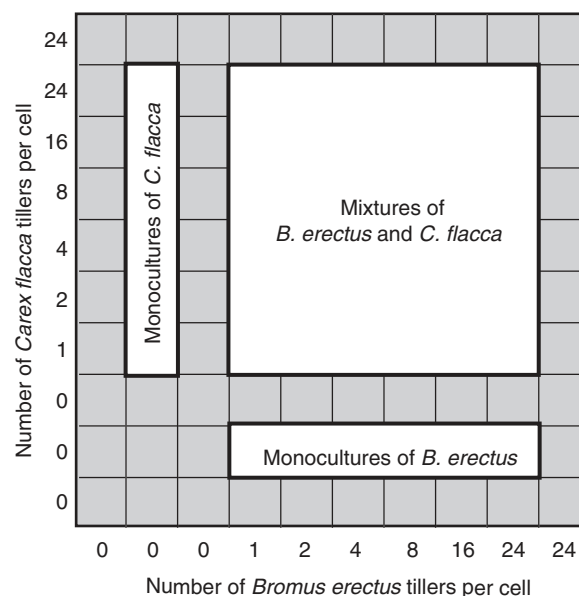


Fig. 1 Illustration of an experimental quadrant used in the experiment testing for effects of elevated [CO₂] and intra- and interspecific planting densities in *Bromus erectus* and *Carex flacca*. Cells were 8 × 8 cm². Gray cells were used as buffer.

Our planting scheme makes use of the fan design proposed by Nelder (1962). This design is highly space-efficient but does create statistical dependencies between treatments (different densities within 'fans' are not randomized). Nevertheless, the design allows the estimation of statistical parameters of density dependence in single-species (Nelder, 1962) and two-species stands (Assémat & Oka, 1980; Schmid & Harper, 1985).

Measurements

One year after the start of the experiment, in July and August 1998, we counted in each experimental 8 × 8 cm² cell the number of vegetative and reproductive tillers and the number of seeds for each species. Then we harvested the aboveground plant parts of each species per cell by cutting all parts at 3 cm above soil level, and separated it into vegetative parts (i.e. leaves), infructescence stalks, and seeds. We did not separate plant individuals of the same species within cells because it was no longer possible at harvest to assign tillers to planted individuals. We also did not harvest belowground plant parts because it was impossible to extract all roots from the soil and to separate them between the two species. We weighed the harvested material after drying it to constant mass at 80 °C. From these data, we calculated the total aboveground biomass per cell for each species separately and combined.

We calculated the average mass per tiller for each species by dividing the total aboveground biomass by the number of tillers per cell. We calculated the average mass per seed for each species in a cell, by weighing batches of 10 seeds of *B. erectus* and batches of 20 seeds of *C. flacca*, and dividing the mass of each batch by the number of seeds per batch.

Analyses

We analyzed all variables with analysis of variance (sequential sum of squares) according to a split-plot design using the statistical software Genstat (Payne *et al.*, 1993). The design consisted of three blocks (i.e. pairs of FACE and control rings), six plots (i.e. rings), 24 quadrants, and 1158 cells. The [CO₂] effect was tested against the variation among plots, and the effects of densities of *B. erectus* and *C. flacca* were tested against the residual variation (i.e. variation among cells). To assess the functional relationship between planting densities of the two species and their interactions as explanatory terms and each measured trait as dependent variable, we partitioned the sums of squares of density effects and their interactions with [CO₂] into linear, quadratic and remaining (i.e. deviation) components by using polynomial contrasts. For each species, we excluded the cells in which their planting density was 0, thereby reducing the number of cells to 1014 for each species. Before analyses, aboveground biomass, average mass per tiller and total number of seeds of

each species per cell, and the combined biomass per cell were log₁₀ transformed to achieve normality and homogeneity of variance.

Results

Effects of [CO₂] and planting densities of B. erectus and C. flacca on total biomass production

Total aboveground biomass production increased with increasing planting densities of both species to a maximum of about 4000 mg per 8 × 8 cm² cell and tended to decrease again at the highest planting densities (Fig. 2). This is indicated by significant linear and quadratic components of the *Carex*- and *Bromus*-density effects (Table 1). The effects of *Carex* and *Bromus* planting density, however, did not act independently as indicated by their significant interaction (Fig. 2, Table 1). On average, there was no significant effect of [CO₂] on total aboveground biomass but the effect of [CO₂] depended on the planting density of *Carex* (Fig. 2, Table 1). This interaction, however, could not be ascribed to linear or quadratic components of the density gradient (Table 1).

Effects of [CO₂] and intra- and interspecific planting density on biomass and reproduction of B. erectus

Aboveground biomass of *B. erectus* increased asymptotically with intraspecific planting density to about 1500 mg per 8 × 8 cm² cell (Fig. 3a, significant linear

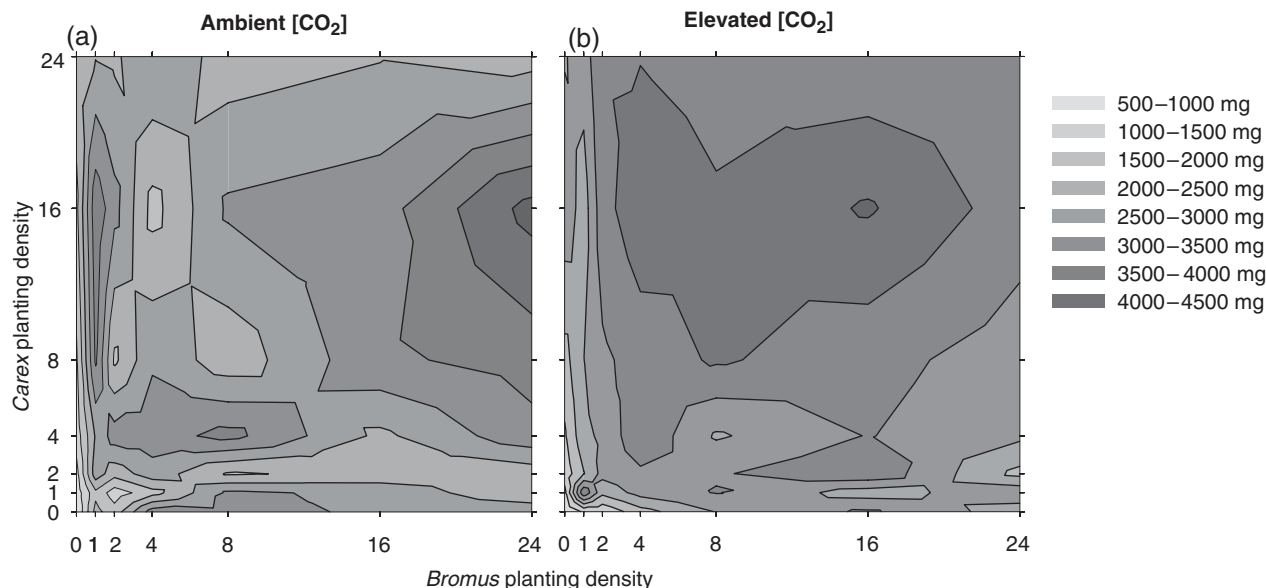


Fig. 2 Combined aboveground biomass [milligram per 8 × 8 cm² cell] of *Bromus erectus* and *Carex flacca* in response to planting densities of both species at (a) ambient and (b) elevated [CO₂]. Contour lines are separated by 500 mg and an increase in shading intensity when passing a contour line indicates an increase in biomass production. The highest biomass yields are shifted toward more equal species frequencies under elevated [CO₂]. The biomass values were back transformed after log₁₀ transformation of the original data.

Table 1 Analysis of variance of the combined aboveground biomass of *Carex flacca* and *Bromus erectus* per 8 × 8 cm² cell

Effect	df	MS	F
Block	2	0.5508	1.31
CO ₂	1	0.2718	0.64
Plot	2	0.4216	0.58
Quadrant	18	0.7299	3.28***
<i>Carex density</i>	6	7.1829	32.28***
Linear	1	18.2049	81.82***
Quadratic	1	13.3790	60.13***
Deviation	3	2.8784	12.94***
<i>Bromus density</i>	6	14.5699	65.48***
Linear	1	19.7947	88.97***
Quadratic	1	21.1148	94.90***
Deviation	4	11.6275	52.26***
CO ₂ × <i>Carex density</i>	6	0.7788	3.50**
Linear	1	0.6858	3.08
Quadratic	1	0.0288	0.13
Deviation	4	0.9896	4.45**
CO ₂ × <i>Bromus density</i>	6	0.2649	1.19
Linear	1	0.0888	0.40
Quadratic	1	0.2551	1.15
Deviation	4	0.3114	1.40
<i>Carex</i> × <i>Bromus density</i>	36	3.3516	15.06***
CO ₂ × <i>Carex</i> × <i>Bromus density</i>	36	0.1614	0.73
Residual	1014	0.2225	

** $P < 0.01$. *** $P < 0.001$.

Plants were grown in a split-plot design at two levels of [CO₂] and at different densities of *C. flacca* and *B. erectus*. Effects of the planting densities of *C. flacca* and *B. erectus* and their interactions with [CO₂] were separated into linear and non-linear components with polynomial contrasts. The combined aboveground biomass was log₁₀ transformed before analysis.

and quadratic components of the intraspecific-density effect in Table 2), and indicates that intraspecific competition increases at higher planting densities and reduces biomass production per individual of *B. erectus*. Aboveground biomass of *B. erectus* decreased with interspecific planting density to about 500 mg per 8 × 8 cm² cell (Fig. 3a, significant linear component of the interspecific-density effect in Table 2), and indicates that biomass production of *B. erectus* is decreased by interspecific competition. There was no significant interaction between the effects of intra- and interspecific competition. On average, there was no significant effect of [CO₂] but the effects of intra- and interspecific competition depended on [CO₂] (Fig. 3a, Table 2). These interactions, however, could not be ascribed to linear or quadratic components of the density gradients (Table 2).

One year after the start of the experiment, the number of tillers of *B. erectus* per 8 × 8 cm² cell had more than

doubled at the low planting densities and decreased by about 50% at the highest one, to some degree leveling out the initial differences (Fig. 3c). Nevertheless, tiller number was still positively related to intraspecific planting density as indicated by the significant linear component of the intraspecific-density effect (Table 2) but the relation was asymptotic as indicated by the significant quadratic component of the intraspecific-density effect (Table 2). The number of tillers of *B. erectus* per cell decreased with increasing planting density of *C. flacca* as indicated by a significant linear component of the interspecific-density effect (Fig. 3c, Table 2) but the slope of this decrease was less steep at higher planting densities as indicated by a significant quadratic component of the interspecific-density effect (Table 2). On average, the number of tillers per cell significantly decreased by 8.5% under elevated [CO₂]. This negative effect of [CO₂], however, was not apparent at intermediate planting densities of *B. erectus* (Fig. 3, significant quadratic component of the CO₂ × intraspecific-density interaction in Table 2).

The average mass per tiller of *B. erectus* was not significantly affected by intra- and interspecific planting density (Fig. 3e, Table 2). Overall, there was also no significant effect of [CO₂] on mass per tiller (Fig. 3e, Table 2). However, there was a significant [CO₂] × intraspecific-density interaction but this could not be ascribed to linear or quadratic components of the density gradient (Fig. 3e, Table 2). There was no significant interaction between [CO₂] and interspecific planting density (Fig. 3e, Table 2).

The number of seeds of *B. erectus* produced per cell was significantly higher at intermediate intraspecific planting density than at low and high ones (Fig. 3g) as indicated by a significant quadratic component of the intraspecific-density effect (Table 2). On the other hand, it decreased with interspecific planting density from about 20 to 5 per 8 × 8 cm² cell (Fig. 3g, Table 2). On average, there was no significant effect of [CO₂] on the number of seeds but the effect of intraspecific planting density depended on [CO₂] (Fig. 3g, Table 2). This interaction, however, could not be ascribed to linear or quadratic components of the intraspecific-density gradient (Table 2).

The average mass per seed of *B. erectus* was not significantly affected by intraspecific planting density but decreased significantly with increasing interspecific planting density (Fig. 3i, significant linear component of the interspecific density effect in Table 2). The effect of interspecific competition, however, depended on the level of intraspecific planting density as indicated by their significant interaction (Table 2). On average, the mass per seed was not significantly affected by [CO₂] but the negative effect of interspecific competition on

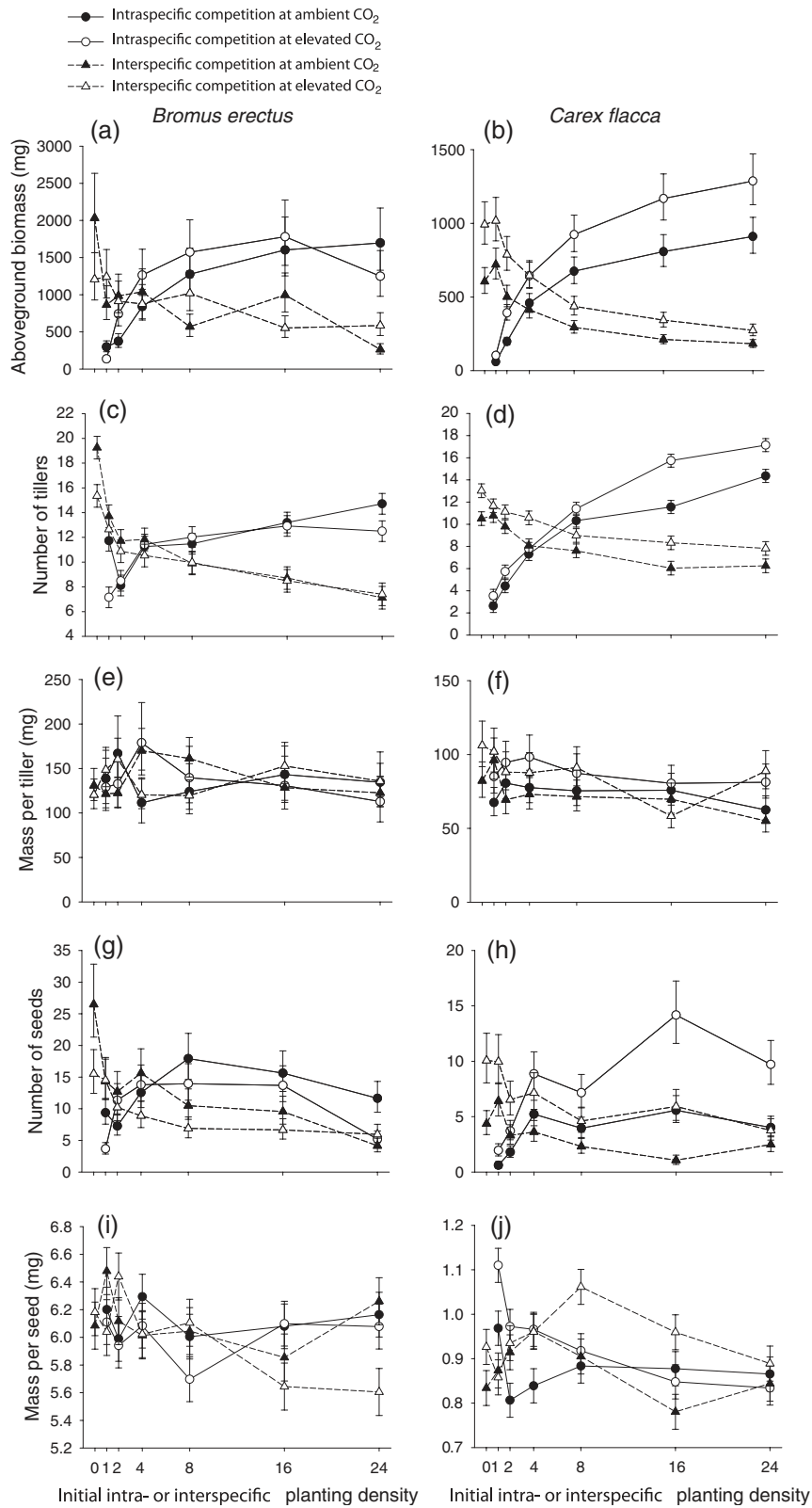


Fig. 3 Aboveground biomass (milligram per $8 \times 8 \text{ cm}^2$ cell), number of tillers (per $8 \times 8 \text{ cm}^2$ cell), average mass per tiller (mg), number of seeds (per $8 \times 8 \text{ cm}^2$ cell) and average mass per seed (mg) (means \pm SEs) of *Bromus erectus* and *Carex flacca* in response to intra- (circles and solid lines) and interspecific (triangles and dashed lines) planting densities at ambient (closed symbols) and elevated (open symbols) [CO₂].

Table 2 Analyses of variance (*F*-values) of fitness measures of *Bromus erectus*

Effect	df	Aboveground biomass	Number of tillers	Average mass per tiller	Number of seeds	Average mass per seed
Block	2	0.79	5.28	1.79	8.70	4.69
CO ₂	1	0.07	52.82*	0.00	6.42	0.56
Plot	2	1.00	0.03	0.69	0.03	0.64
Quadrant	18	2.53***	2.56***	2.63***	19.48***	7.66***
Intraspecific density	5	28.12***	10.20***	0.58	6.35***	2.09
Linear	1	70.04***	39.66***	1.47	0.37	0.10
Quadratic	1	45.93***	4.81*	0.10	27.44***	1.98
Deviation	3	8.21***	2.18	0.44	1.31	2.79*
Interspecific density	6	6.38***	22.47***	0.28	7.38***	3.62**
Linear	1	32.14***	92.29***	0.02	37.36***	12.71***
Quadratic	1	0.00	15.26***	1.02	1.31	3.16
Deviation	4	1.53	6.82***	0.16	1.40	1.47
CO ₂ × intraspecific density	5	2.87*	2.47*	2.30*	2.73*	0.44
Linear	1	0.59	0.00	1.07	1.96	0.14
Quadratic	1	2.71	5.39*	1.67	2.16	0.17
Deviation	3	3.69*	2.32	2.92*	3.17*	0.62
CO ₂ × interspecific density	6	2.61*	1.03	1.83	0.97	3.00**
Linear	1	2.19	2.73	0.25	1.93	7.76**
Quadratic	1	0.76	0.94	1.43	1.67	2.51
Deviation	4	3.18*	0.63	2.32	0.55	1.93
Intra- × interspecific density	30	0.82	1.33	0.92	0.82	2.17**
CO ₂ × intra- × interspecific density	30	1.22	0.84	0.71	0.98	1.45
Residual	874 [†]	(0.7529)	(69.43)	(0.2273)	(0.6187)	(133.6)

* $P < 0.05$. ** $P < 0.01$. *** $P < 0.001$.

[†]Residual df is 902, 828, 881 and 284 for number of tillers, average mass per tiller, number of seeds and average mass per seed, respectively.

Plants were grown in a split-plot design at two levels of [CO₂] and at different levels of intraspecific and interspecific (other species: *Carex flacca*) planting densities. Effects of intra- and interspecific planting densities and their interactions with [CO₂] were separated into linear and nonlinear components with polynomial contrasts. Residual MS are given between parentheses. Aboveground biomass, average mass per tiller and number of seeds were log₁₀ transformed before analysis.

the mass per seed was strongest under elevated [CO₂] where it decreased from about 6.3 mg at the lowest densities to about 5.6 mg at the highest one (Fig. 3i, significant linear component of the CO₂ × interspecific-density interaction in Table 2).

Effects of [CO₂] and intra- and interspecific planting density on biomass and reproduction of C. flacca

Aboveground biomass of *C. flacca* increased asymptotically with intraspecific planting density to about 1000 mg per 8 × 8 cm² cell (Fig. 3b, significant linear and quadratic components of the intraspecific-density effect in Table 3), indicating that intraspecific competition increases also at higher planting densities in *C. flacca*. Aboveground biomass of *C. flacca* decreased asymptotically with interspecific planting density to about 200 mg per 8 × 8 cm² cell (Fig. 3b, significant linear and quadratic components of the interspecific-

density effect in Table 3), and indicates that biomass production of *C. flacca* is decreased by interspecific competition. Moreover, intra- and interspecific competition did not act independently as indicated by their significant interaction (Table 3). On average, aboveground biomass was significantly increased by 54% under elevated [CO₂] (Fig. 3b, Table 3) and there were no significant interactions between [CO₂] and intra- or interspecific planting density (Table 3).

One year after the start of the experiment, the number of tillers of *C. flacca* per cell had doubled at the low planting densities and decreased by about 35% at the highest planting density such that tiller density was still strongly positively related to intraspecific planting density (Fig. 3d, significant linear and quadratic components of the intraspecific-density effect in Table 3). The number of tillers decreased asymptotically with increasing interspecific planting density to about 8 per 8 × 8 cm² cell (Fig. 3d, significant linear and quadratic

Table 3 Analyses of variance (*F*-values) of fitness measures of *Carex flacca*

Effect	df	Aboveground biomass	Number of tillers	Average mass per tiller	Number of seeds	Average mass per seed
Block	2	20.64*	8.96	0.40	18.63	1.86
CO ₂	1	38.57*	9.56	1.14	162.73**	2.091
Plot	2	0.06	0.50	1.13	0.01	2.48
Quadrant	18	13.44***	9.31***	11.90***	16.45***	6.06***
<i>Intraspecific density</i>	5	106.55***	228.79***	2.01	16.37***	20.90***
Linear	1	306.09***	1032.44***	4.82*	35.07***	47.14***
Quadratic	1	122.00***	90.99***	1.19	27.52***	10.13***
Deviation	3	34.88***	6.84***	1.35	6.43***	15.74***
<i>Interspecific density</i>	6	25.24***	28.99***	6.13***	4.81***	9.35***
Linear	1	135.57***	143.89***	23.38***	19.21***	4.61*
Quadratic	1	12.00***	27.12***	5.25*	6.12*	19.49***
Deviation	4	0.96	0.74	2.04	0.88	8.00***
CO ₂ × <i>intraspecific density</i>	5	0.57	4.66***	0.44	0.29	8.84***
Linear	1	0.91	13.82***	0.000	0.87	37.83***
Quadratic	1	0.64	1.33	1.37	0.00	4.70*
Deviation	3	0.44	2.71*	0.27	0.20	0.56
CO ₂ × <i>interspecific density</i>	6	0.06	0.84	2.68*	0.94	5.69*
Linear	1	0.00	0.00	0.43	0.03	4.29*
Quadratic	1	0.00	0.11	5.81*	1.71	11.85***
Deviation	4	0.09	1.24	2.47*	0.98	4.49**
Intra- × interspecific density	30	2.17***	1.17	0.56	1.01	6.55**
CO ₂ × intra- × interspecific density	30	0.53	0.64	0.84	0.86	4.07***
Residual	888 [†]	(0.2925)	(18.00)	(0.1003)	(0.6217)	(14.85)

* $P < 0.05$. ** $P < 0.01$. *** $P < 0.001$.

[†]Residual df is 902, 847, 897 and 179 for number of tillers, average mass per tiller, number of seeds and average mass per seed, respectively.

Plants were grown in a split-plot design at two levels of [CO₂] and at different levels of intraspecific and interspecific (other species: *Bromus erectus*) planting densities. Effects of intra- and interspecific planting densities and their interactions with [CO₂] were separated into linear and non-linear components with polynomial contrasts. Residual MS are given between parentheses. Aboveground biomass, average mass per tiller and number of seeds were log₁₀ transformed before analysis.

components of the interspecific density effect in Table 3). On average, the number of tillers per cell was increased by 21% under elevated [CO₂] but this effect was only marginally significant ($P = 0.091$, Table 3), which is not surprising considering the low statistical power of the test. However, the positive effect of [CO₂] on the number of tillers was strongest at high intraspecific planting densities (Fig. 3d, significant linear component of the CO₂ × intraspecific-density interaction in Table 3).

The average mass per tiller of *C. flacca* decreased with increasing intraspecific planting density from about 85 to 75 mg (Fig. 3f) but this effect was only marginally significant ($P = 0.075$, Table 3f). The mass per tiller decreased asymptotically with increasing interspecific planting density from about 90 to 75 mg (Fig. 3f, significant linear and quadratic components of the interspecific-density effect in Table 3). On average, there was no significant effect of [CO₂] on mass per tiller but the mass per tiller was higher under elevated [CO₂] at low

and high interspecific planting densities (Fig. 3f, significant quadratic component of the [CO₂] × interspecific-density interaction in Table 3). There was no significant interaction between [CO₂] and intraspecific planting density (Fig. 3f, Table 3).

The number of seeds produced by *C. flacca* increased asymptotically with increasing intraspecific planting density from about 2 to a maximum of 14 per 8 × 8 cm² cell (Fig. 3h, significant linear and quadratic components of the intraspecific-density effect in Table 3). Seed production decreased asymptotically with increasing interspecific planting density from about 8 to 3 per 8 × 8 cm² cell (Fig. 3h, significant linear and quadratic components of the interspecific-density effect in Table 3). On average, seed production of *C. flacca* was significantly increased by 112% under elevated [CO₂] (Fig. 3h, Table 3). There were no significant interactions between [CO₂] and intra- or interspecific planting density (Table 3).

The average mass per seed of *C. flacca* decreased asymptotically with increasing intraspecific planting

density from about 1.1 to 0.9 mg (Fig. 3j, significant linear and quadratic components of the intraspecific-density effect in Table 3). Although the heaviest seeds were produced at intermediate interspecific planting densities, on average, the mass per seed decreased slightly with increasing interspecific planting density (Fig. 3j, significant linear and quadratic components of the interspecific-density effect in Table 3). Moreover, the effects of intra- and interspecific planting density were not independent from each other (significant intra- × interspecific density interaction in Table 3). On average, the mass per seed was not significantly affected by [CO₂]. However, the mass per seed was increased by elevated [CO₂] at low intraspecific planting densities (+15% at the lowest planting density) and slightly decreased at high intraspecific planting densities (−4% at the highest planting density; Fig. 3j, significant linear and quadratic components of the CO₂ × intraspecific-density interaction in Table 3). Moreover, the mass per seed was increased by elevated [CO₂] by about 20% at intermediate interspecific planting densities but not or to a lesser extent at the lowest and highest planting densities (Fig. 3j, significant linear and quadratic components of the CO₂ × interspecific-density interaction in Table 3). Furthermore, there was a significant three-way interaction between [CO₂], intra- and interspecific planting density (Table 3).

Discussion

Changes in productivity under elevated [CO₂]

Our study showed that after 1 year aboveground biomass production of *C. flacca* was increased under elevated [CO₂] by 54% while the biomass of *B. erectus* was not affected by [CO₂]. However, because *C. flacca* produced the smaller proportion (35%) of the total biomass, the combined biomass of the whole stand was not significantly increased under elevated [CO₂]. Other studies also report that although the biomass of single species may increase under elevated [CO₂], the biomass of the whole community often does not respond (Bazzaz & Garbutt, 1988; Ramseier *et al.*, 2005) or is mainly driven by the response of one or a few species (Bernston *et al.*, 1998). Although 1 year of growth is relatively long compared with many other studies, it could be that biomass responses to elevated [CO₂] only become apparent after a longer time (Warwick *et al.*, 1998; Stöcklin *et al.*, 1998).

Aboveground biomass of *B. erectus* was not significantly affected by [CO₂] but the number of tillers per cell decreased on average by 8.5%, suggesting that the tillers got larger. Overall, however, there was no significant effect of [CO₂] on the average mass per

B. erectus tiller. For *C. flacca*, on the other hand, the number of tillers increased in response to elevated [CO₂] though to a lesser extent (21.2%) than the aboveground biomass (54.0%). This also suggests that tillers of *C. flacca* grew larger under elevated [CO₂]. However, a positive effect of elevated [CO₂] on mass per *C. flacca* tiller was only apparent at low and high interspecific densities while the reverse was true at an intermediate density. Overall, these results indicate that for both species the relative allocation to number and size of vegetative offspring is not significantly changed under elevated [CO₂].

B. erectus neither increased seed production nor the average mass per seed under elevated [CO₂] while *C. flacca* more than doubled the number of seeds in response to elevated [CO₂]. The smaller magnitude of the increase in number of tillers than in seed production in *C. flacca* suggests a shift from vegetative to sexual reproduction under elevated [CO₂] as has also been found for other species such as *Ambrosia artemisiifolia* (Stinson & Bazzaz, 2006). In the latter study, this was a consequence of reduced competition under elevated [CO₂] resulting in more of the small plants to reproduce. The mass of individual seeds of *C. flacca* was not affected by elevated [CO₂]. Similarly, Garbutt & Bazzaz (1984) found that the fruit mass of *Datura stramonium* also increased under elevated [CO₂] and that the seed size was not affected. For *Abutilon theophrasti*, on the other hand, they found that seed number was lower but individual seed mass was higher for plants grown at elevated [CO₂]. This shows that sexual reproductive characteristics of different species can be affected quite differently by elevated [CO₂]. Such changes in reproductive allocation in response to elevated [CO₂] could be a consequence of plants being along different parts of their allometric trajectories or having changed their allometric trajectories in response to elevated [CO₂] (He & Bazzaz, 2002; Stinson & Bazzaz, 2006). Because we have not measured reproductive allocation at the individual plant level, we cannot differentiate between these two options. Nevertheless, the change in reproductive allocation in response to elevated [CO₂] suggests that under elevated [CO₂] community composition is likely to change. These changes, however, are likely to depend on the degree of changes in intra- and interspecific competition.

Effects of intraspecific planting density and changes therein under elevated [CO₂]

Aboveground biomass of *C. flacca* and *B. erectus* increased asymptotically with increasing intraspecific planting density which is in line with the rule of constant final yield (Kira *et al.*, 1953). This suggests that

the rule of constant yield does not only apply to monocultures but also to mixtures (He *et al.*, 2005). On average, the number of tillers increased at planting densities in the range of one to eight tillers per $8 \times 8 \text{ cm}^2$ cell, while self-thinning at higher planting densities resulted in lower numbers of tillers per cell than the original planting densities. Overall, this resulted in an asymptotic increase in the number of tillers per cell with increasing intraspecific planting density for both species.

The number of seeds of *C. flacca* per cell also increased asymptotically with increasing intraspecific planting density. However, concomitantly there was an asymptotic decrease in the average mass per seed, indicating that under high intraspecific planting densities the overall seed number remained constant but at a cost of individual seed mass. For *B. erectus*, there was also an asymptotic increase in the number of seeds with increasing intraspecific planting density but only up to a planting density of 16 tillers per $8 \times 8 \text{ cm}^2$ cell after which it decreased again. Such a hump-shaped relation between seed production and density has also been found for *Erophila verna* (Symonides *et al.*, 1986) and *Abutilon theophrasti* (Bazzaz *et al.*, 1992) and indicates overcompensating density dependence (i.e. the increase in seed production due to a larger number of individuals at high densities is overcompensated by the reduction in individual seed production; Silvertown, 1987). The individual seed mass of *B. erectus*, however, did not decrease with increasing intraspecific planting density, indicating that *B. erectus*, in contrast to *C. flacca*, does not maintain a high seed production at high intraspecific planting densities at a cost to individual seed mass.

In general, plants are more stimulated by elevated $[\text{CO}_2]$ when grown individually or at very low density than when grown in dense monocultures (Navas, 1998) or when grown for a short time period or at high nutrient levels (Körner, 1999). When experiments are done under more realistic conditions, with interspecific competition and for a longer time period, however, results might be different. Indeed, the positive effect of elevated $[\text{CO}_2]$ on the number of tillers of *C. flacca* per cell was largest at high intraspecific planting densities rather than at low planting densities.

For *B. erectus*, there were also significant interactions between elevated $[\text{CO}_2]$ and intraspecific planting density for aboveground biomass and for the number of tillers and seeds but these interactions could not be attributed to linear components. For the number of tillers of *B. erectus* the interaction was a consequence of negative effects of elevated $[\text{CO}_2]$ at both low and high intraspecific planting densities but not at intermediate ones. Although the causes of this pattern are elusive, it exemplifies the importance of studying the

effect of elevated $[\text{CO}_2]$ at a range of planting densities. Similarly, Bazzaz *et al.* (1992) found that the positive effect of elevated $[\text{CO}_2]$ on the number of fruiting plants of *Abutilon theophrasti* was highest at intermediate densities. For aboveground biomass and the number of seeds of *B. erectus*, however, the effect of elevated $[\text{CO}_2]$ depended neither on linear nor on quadratic components of the density gradient. This indicates that even if the effect of elevated $[\text{CO}_2]$ is tested over a large range of planting density extrapolation of the results to other planting densities may be difficult.

Effects of interspecific planting density and changes therein under elevated $[\text{CO}_2]$

Interspecific planting density had a negative effect on biomass and on vegetative and sexual reproduction for both species. For *C. flacca*, the negative effect of interspecific planting density was asymptotic, except for the average mass per seed, which showed an optimum at intermediate densities. On the other hand, the negative effect of interspecific planting density on aboveground biomass and seed production of *B. erectus* was linear. Presumably, as a consequence of the overall lower biomass of tillers of *C. flacca*, a higher planting density is required before a nonlinear effect on *B. erectus* becomes apparent.

For both species, elevated $[\text{CO}_2]$ modified the consequences of interspecific planting density for the average mass per seed but in different ways. For *B. erectus*, there was a strong negative effect of elevated $[\text{CO}_2]$ at high interspecific planting densities, while for *C. flacca*, there was a strong positive effect at intermediate interspecific planting densities. The latter, however, was not independent of the intraspecific planting density as indicated by a significant $[\text{CO}_2] \times \text{intraspecific-density} \times \text{interspecific-density}$ interaction. Moreover, there was also a significant interaction between $[\text{CO}_2]$ and interspecific competition on biomass of *B. erectus*. This, however, could not be ascribed to linear or quadratic components of the density gradient and indicates that the biomass response of *B. erectus* to elevated $[\text{CO}_2]$ at different interspecific densities is difficult to predict.

Conclusions

For accurate predictions of the effects of elevated $[\text{CO}_2]$ on biodiversity due to changes in competitive interactions, plants should be grown at a range of densities and frequencies with other species. Our study is one of the most detailed assessments in this regard and shows that the responses of *B. erectus* and *C. flacca* to elevated $[\text{CO}_2]$ depend on both intra- and interspecific planting density. Because density effects often did not follow

simple functional relationships, precise prediction of responses to elevated [CO₂] of realistic plant communities with varying local densities and frequencies of these two interacting species are highly complex. At a crude level, our experiment allows us to predict that the increase in biomass and number of seeds of *C. flacca* and the absence of such effects and even a decrease in number of tillers of *B. erectus* in response to elevated [CO₂] are likely to lead over the coming decades to an increased abundance of *C. flacca* relative to *B. erectus* in communities of calcareous grasslands in Europe.

Acknowledgements

We thank the group of Prof. Nösberger, in particular Andreas Lüscher, for allowance to use the FACE facility in Eschikon, and Andrea Meyer, Rolf Gall, Carmen Gaadt-Stephan, Ursula Hauser, Markus Schmid, Nadine Salzmann, Beatrice Neff, Marcel Grob, Horst Machguth, Ilja, Philipp Kocyan, Thomas Pfluger, Gillian Rutherford-Rauh, Felix Eichenberger, Angelika von Förster, Sascha Oehler, Isabel Reding, Rahel Schmid, Daniel Schmidt, Patrick Lang, Andreas Rappo and Elvira Zingg for practical assistance. This project was supported by Grant No. 5001-44628 of the Swiss National Science Foundation.

References

- Assémat L, Oka HI (1980) Neighbor effects between rice (*Oryza sativa* L.) and barnyard grass (*Echinochloa crus-galli* Beauv) strains. 1. Performance in mixture and aggressiveness as influenced by planting density. *Oecologia Plantarum*, **15**, 371–393.
- Bazzaz FA, Ackerly DD, Woodward FI *et al.* (1992) CO₂ enrichment and dependence of reproduction on density in an annual plant and a simulation of its population dynamics. *Journal of Ecology*, **80**, 643–651.
- Bazzaz FA, Garbutt K (1988) The response of annuals in competitive neighborhoods: effects of elevated CO₂. *Ecology*, **69**, 937–946.
- Bernston GM, Rajakaruna N, Bazzaz FA (1998) Growth and nitrogen uptake in experimental community of annuals exposed to elevated atmospheric CO₂. *Global Change Biology*, **4**, 607–626.
- Diaz S (1995) Elevated CO₂ responsiveness, interactions at the community level and plant functional types. *Journal of Biogeography*, **22**, 289–295.
- Diaz S, Fraser LH, Grime JP *et al.* (1998) The impact of elevated CO₂ on plant–herbivore interactions: experimental evidence of moderating effects at the community level. *Oecologia*, **117**, 177–186.
- Dukes JS (2002) Comparison of the effect of elevated to elevated CO₂ on an invasive species (*Centaurea solstitialis*) in monoculture and community settings. *Plant Ecology*, **160**, 225–234.
- Ellenberg H (1986) *Vegetation Ecology of Central Europe*. Cambridge University Press, Cambridge.
- Firbank LG, Watkinson AR, Norton LR *et al.* (1995) Plant populations and global environmental change: the effects of different temperature, carbon dioxide and nutrient regimes on density dependence in populations of *Vulpia ciliata*. *Functional Ecology*, **9**, 432–441.
- Fischer M, Stöcklin J (1997) Local extinction of plants in remnants of extensively used calcareous grasslands 1950–1985. *Conservation Biology*, **11**, 727–737.
- Garbutt K, Bazzaz FA (1984) The effect of elevated CO₂ on plants. III. Flower, fruit and seed production and abortion. *New Phytologist*, **98**, 433–446.
- He J-S, Bazzaz FA (2002) Density-dependent responses of reproductive allocation to elevated atmospheric CO₂ in *Phytolacca Americana*. *New Phytologist*, **157**, 229–239.
- He J-S, Wolfe-Bellin KS, Schmid B *et al.* (2005) Density may alter diversity–productivity relationships in experimental plant communities. *Basic and Applied Ecology*, **6**, 505–517.
- Hely SEL, Roxburgh SH (2005) The interactive effects of elevated CO₂, temperature and initial size on growth and competition between a native C₃ and invasive C₃ grass. *Plant Ecology*, **177**, 85–98.
- Hendrey GR, Lewin KF, Nagy J (1993) Free air carbon dioxide enrichment: development, progress, results. *Vegetatio*, **104–105**, 17–31.
- Hikosaka K, Onoda Y, Kinugasa T *et al.* (2005) Plant responses to elevated CO₂ concentrations at different scales: leaf, whole plant, canopy, and population. *Ecological Research*, **20**, 243–253.
- Hunt R, Hand DW, Hannah MA *et al.* (1991) Response to CO₂ enrichment in 27 herbaceous species. *Functional Ecology*, **5**, 410–421.
- IPCC (2001) *Climatic Change 2001: Synthesis Report. Summary for Policymakers*. Intergovernmental Panel on Climate Change, Geneva.
- Inouye BD (2001) Response surface experimental designs for investigating interspecific competition. *Ecology*, **82**, 2696–2706.
- Keeling CD (1993) Global observations of atmospheric CO₂. In: *The Global Carbon Cycle* (ed. Heimann M), pp. 1–29. Springer-Verlag, Berlin.
- Kira T, Ogawa H, Sakazaki N (1953) Intraspecific competition among higher plants. I. Competition–yield–density interrelationships in regularly dispersed populations. *Journal of the Institute of Polytechnics, Osaka City University, Series D*, **7**, 1–14.
- Körner C (1995) Towards a better experimental basis for upscaling plant responses to elevated CO₂ and climate warming. *Plant, Cell and Environment*, **18**, 1101–1110.
- Körner C (1999) Biologischen Folgen der CO₂-Erhöhung. *Biologie in unserer Zeit*, **6**, 353–363.
- Körner C, Bazzaz FA (eds) (1996) *Carbon Dioxide, Populations, and Communities. Physiological Ecology Series*. Academic Press, San Diego.
- Law R, Watkinson AR (1987) Response-surface analysis of two-species competition: an experiment on *Phleum arenarium* and *Vulpia fasciculata*. *Journal of Ecology*, **75**, 871–886.
- Leadley PW, Körner C (1996) Effects of elevated CO₂ on plant species dominance in a highly diverse calcareous grassland. In: *Carbon Dioxide, Populations, and Communities. Physiological Ecology Series* (eds Körner C, Bazzaz FA), pp. 159–175. Academic Press, San Diego.
- Leadley PW, Stöcklin J (1996) Effects of elevated CO₂ on model calcareous grasslands: community, species and genotype level responses. *Global Change Biology*, **2**, 389–397.

- Navas M-L (1998) Individual species performance and response of multi-specific communities to elevated CO₂: a review. *Functional Ecology*, **12**, 721–727.
- Navas M-L, Garnier E, Austin MP *et al.* (1999) Effect of competition on the responses of grasses and legumes to elevated atmospheric CO₂ along a nitrogen gradient: differences between isolated plants, monocultures and multi-species mixtures. *New Phytologist*, **143**, 323–331.
- Nelder JA (1962) New kinds of systematic designs for spacing experiments. *Biometrics*, **18**, 283–307.
- Payne RW, Lane PW, Digby PGN *et al.* (1993) *Genstat 5 Reference Manual*. Clarendon Press, Oxford.
- Peters RL, Lovejoy TL (eds) (1992) *Global Warming and Biological Diversity*. Yale University Press, New Haven.
- Poorter H, Navas M-L (2003) Plant growth and competition at elevated CO₂: on winners, losers and functional groups. *New Phytologist*, **157**, 175–198.
- Poorter H, Roumet C, Campbell BD (1996) Interspecific variation in the growth response of plants to elevated CO₂: a search of functional types. In: *Carbon Dioxide, Populations, and Communities. Physiological Ecology Series* (eds Körner C, Bazzaz FA), pp. 375–412. Academic Press, San Diego.
- Ramseier D, Connolly J, Bazzaz FA (2005) Carbon dioxide regime, species identity and influence of species initial abundance as determinants of change in stand biomass composition in five-species communities: an investigation using a simplex design and RGRD analysis. *Journal of Ecology*, **93**, 502–511.
- Schmid B, Birrer A, Lavigne C (1996) Genetic variation in the response of plant populations to elevated CO₂ in a nutrient-poor, calcareous grassland. In: *Carbon Dioxide, Populations and Communities. Physiological Ecology Series* (eds Körner C, Bazzaz FA), pp. 31–50. Academic Press, San Diego.
- Schmid B, Harper JL (1985) Clonal growth in grassland perennials. I. Density and pattern dependent competition between plants with different growth form. *Journal of Ecology*, **73**, 793–808.
- Silvertown J (1987) *Introduction to Plant Population Ecology*. Longman, Harlow.
- Steinger T, Lavigne C, Birrer A *et al.* (1997) Genetic variation in response to elevated CO₂ in three grassland perennials – a field experiment with two competition regimes. *Acta Oecologia*, **18**, 263–268.
- Stinson KA, Bazzaz FA (2006) CO₂ enrichment reduces reproductive dominance in competing stands of *Ambrosia artemisiifolia* (common ragweed). *Oecologia*, **147**, 155–163.
- Stöcklin J, Schweizer K, Körner C (1998) Effects of elevated CO₂ and phosphorus addition on productivity and community composition of intact monoliths from calcareous grassland. *Oecologia*, **116**, 50–56.
- Strain BR, Bazzaz FA (1983) Terrestrial plant communities. In: *CO₂ and Plants. AAAS Selected Symposium 84* (ed. Lemon ER), pp. 177–222. West View Press, Boulder.
- Symonides E, Silvertown J, Andreassen V (1986) Population cycles caused by overcompensating density-dependence in an annual plant. *Oecologia*, **71**, 156–158.
- van Kleunen M, Fischer M, Schmid B (2001) Effects of intraspecific competition on size variation and reproductive allocation in a clonal plant. *Oikos*, **94**, 515–524.
- van Kleunen M, Fischer M, Schmid B (2002) Experimental life-history evolution: selection on the allocation to sexual reproduction and its plasticity in a clonal plant. *Evolution*, **56**, 2168–2177.
- Warwick KR, Taylor G, Blum H (1998) Biomass and compositional changes occur in chalk grassland turves exposed to elevated CO₂ for two seasons in FACE. *Global Change Biology*, **4**, 375–385.
- Wayne PM, Carnelli AL, Connolly J *et al.* (1999) The density dependence of plant responses to elevated CO₂. *Journal of Ecology*, **87**, 183–192.
- Willems JH (1992) Phytosociological and geographical survey of *Mesobromion* communities in western Europe. *Vegetatio*, **48**, 227–240.
- Zoller H (1954) Die Arten der *Bromus erectus* Wiesen des Schweizer Juras. *Veröffentlichungen des Geobotanischen Institutes ETH, Stiftung Rübel, Zürich*, **28**, 1–283.